Article

Cell Reports

Macrophage Death following Influenza Vaccination Initiates the Inflammatory Response that Promotes Dendritic Cell Function in the Draining Lymph Node

Graphical Abstract

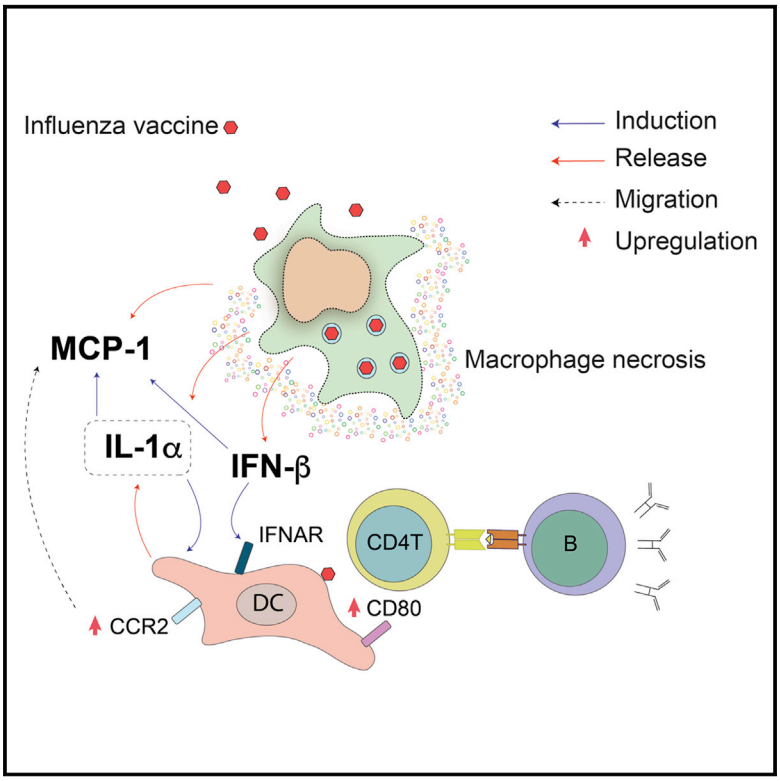

Authors

Nikolaos Chatziandreou, Yagmur Farsakoglu, Miguel Palomino-Segura, ..., Antonio Lanzavecchia, Michael C. Carroll, Santiago F. Gonzalez

Correspondence

santiago.gonzalez@irb.usi.ch

In Brief

The mechanism by which inflammation influences the antibody response to vaccines is unclear. Chatziandreou et al. found that lymph node macrophages are key players in the initiation of the IL-1α-mediated inflammatory response that follows influenza vaccination.

Highlights

- Lymph node macrophages undergo necrosis after vaccination
- Subcapsular sinus macrophage disappearance is mediated by TLR7
- Macrophage death induces the activation and relocation of CD11b^{+} dendritic cells
- IL-1α-mediated inflammation is essential for B cell responses

Chatziandreou et al., 2017, Cell Reports *18*, 2427–2440
March 7, 2017 © 2017 The Author(s).
http://dx.doi.org/10.1016/j.celrep.2017.02.026

CellPress

Cell Reports
Article

OPEN ACCESS
CellPress

Macrophage Death following Influenza Vaccination Initiates the Inflammatory Response that Promotes Dendritic Cell Function in the Draining Lymph Node

Nikolaos Chatziandreou,[1,9] Yagmur Farsakoglu,[1,9] Miguel Palomino-Segura,[1] Rocco D'Antuono,[1] Diego Ulisse Pizzagalli,[1,2] Federica Sallusto,[1,3] Veronika Lukacs-Kornek,[4] Mariagrazia Uguccioni,[1,5] Davide Corti,[6] Shannon J. Turley,[7] Antonio Lanzavecchia,[1,3] Michael C. Carroll,[8] and Santiago F. Gonzalez[1,10,*]

[1]Institute for Research in Biomedicine, Università della Svizzera Italiana, via Vincenzo Vela 6, 6500 Bellinzona, Switzerland
[2]Institute of Computational Science, Università della Svizzera Italiana, via G. Buffi 13, 6900 Lugano, Switzerland
[3]Institute for Microbiology, ETH Zurich, Wolfgang-Pauli-Strasse 10, 8093 Zurich, Switzerland
[4]Department of Internal Medicine II, Saarland University Medical Centre, 66424 Homburg, Germany
[5]Department of Biomedical Sciences, Humanitas University, Via Manzoni 113, 20089 Rozzano-Milan, Italy
[6]Humabs BioMed SA, 6500 Bellinzona, Switzerland
[7]Cancer Immunology, Genentech, South San Francisco, CA 94080, USA
[8]Department of Pediatrics, Harvard Medical School and PCMM, Boston Childrens Hospital, Boston, MA 02115, USA
[9]Co-first author
[10]Lead Contact
*Correspondence: santiago.gonzalez@irb.usi.ch
http://dx.doi.org/10.1016/j.celrep.2017.02.026

SUMMARY

The mechanism by which inflammation influences the adaptive response to vaccines is not fully understood. Here, we examine the role of lymph node macrophages (LNMs) in the induction of the cytokine storm triggered by inactivated influenza virus vaccine. Following vaccination, LNMs undergo inflammasome-independent necrosis-like death that is reliant on MyD88 and Toll-like receptor 7 (TLR7) expression and releases pre-stored interleukin-1α (IL-1α). Furthermore, activated medullary macrophages produce interferon-β (IFN-β) that induces the autocrine secretion of IL-1α. We also found that macrophage depletion promotes lymph node-resident dendritic cell (LNDC) relocation and affects the capacity of CD11b$^+$ LNDCs to capture virus and express co-stimulatory molecules. Inhibition of the IL-1α-induced inflammatory cascade reduced B cell responses, while co-administration of recombinant IL-1α increased the humoral response. Stimulation of the IL-1α inflammatory pathway might therefore represent a strategy to enhance antigen presentation by LNDCs and improve the humoral response against influenza vaccines.

INTRODUCTION

Lymph node macrophages (LNMs) are increasingly subject to investigation with a particular focus on their role in the initiation of the immune response (Gray and Cyster, 2012). LNMs can be classified as subcapsular sinus or medullary macrophages (SSMs and MMs, respectively) according to their anatomical position, expression of different surface markers, and function (Kuka and Iannacone, 2014).

Located in proximity to the lymph node (LN) follicles, SSMs are important components of the innate defense barrier, acting as "flypaper" that prevents the dissemination of lymph-borne pathogens, including viruses (Farrell et al., 2015; Iannacone et al., 2010; Junt et al., 2007; Moseman et al., 2012; Winkelmann et al., 2014), bacteria (Kastenmüller et al., 2012) and parasites (Chtanova et al., 2008). In addition to their role in containing infectious agents, SSMs are known for their capacity to present intact antigen to B cells in the proximal follicles (Carrasco and Batista, 2007; Gaya et al., 2015; Junt et al., 2007; Phan et al., 2007, 2009) and processed antigen to T cells (Hickman et al., 2008). However, the factors that affect the ability of SSMs to recycle intact antigen or process and present it through the major histocompatibility complex (MHC) are yet to be elucidated. Considering the important role of SSMs as antigen-presenting cells (APCs), it has been suggested that they may compete with LN-resident dendritic cells (LNDCs) for antigen capture and presentation to T or B cells (Gonzalez et al., 2010). MMs are known for their high phagocytic capacity that is greater than that of SSMs, and their expression of endosomal degradative enzymes (Kuka and Iannacone, 2014). However, their relevance in the initiation of immune responses is poorly understood mainly due to the lack of suitable methods for their specific depletion.

The ability of LNDCs to capture antigen and induce T cell responses has been documented previously (Gerner et al., 2015; Gonzalez et al., 2010; Hickman et al., 2008; Mempel et al., 2004; Sung et al., 2012; Woodruff et al., 2014). However, the exact location at which antigen presentation occurs and the role that LNMs play in dendritic cell (DC) activation remain

This is an open access article under the CC BY-NC-ND license (http://creativecommons.org/licenses/by-nc-nd/4.0/).

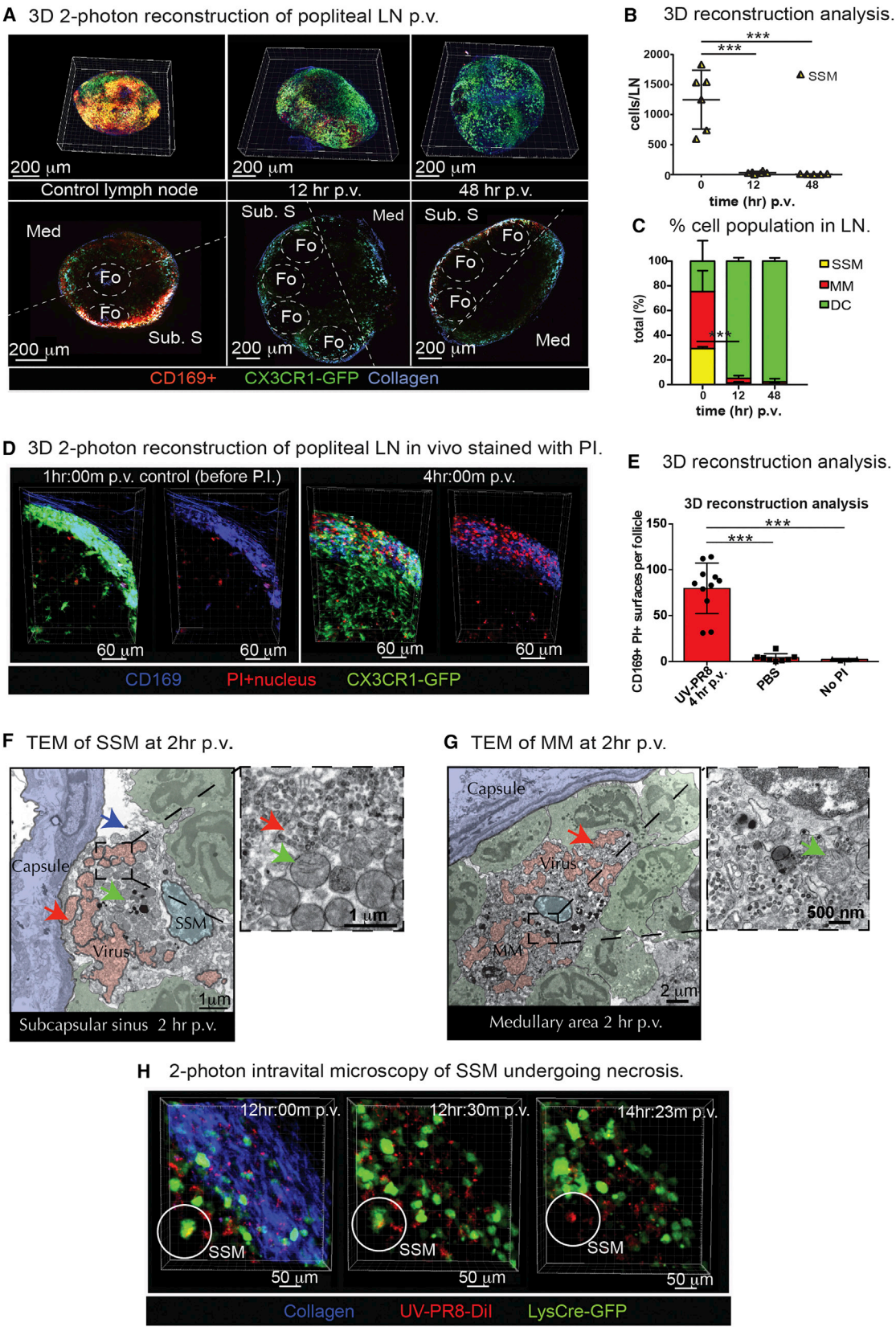

(legend on next page)

controversial. In addition to the well-characterized DC-T cell interaction in the LN cortex (Mempel et al., 2004), recent studies have suggested alternative areas in which this may occur. Woodruff and colleagues (Woodruff et al., 2014) described the relocation of DCs from the paracortex to the medullary area following vaccination. In addition, the interfollicular regions adjacent to the subcapsular sinus appear to be a preferred area for the priming of $CD8^+$ (Gerner et al., 2015; Hickman et al., 2008; Sung et al., 2012) and $CD4^+$ (Gerner et al., 2015; Woodruff et al., 2014) T cells by DCs. Despite the established role of DCs in acquiring antigen, not much is known about the molecular mechanisms that lead to their activation and positioning in lymphoid tissues and the role that LN macrophages have in these processes. Cytokines secreted by macrophages in response to antigen, such as type I interferons (IFNs), have been postulated to participate in the activation of DCs (Moseman et al., 2012; Sung et al., 2012) through a mechanism that involves the induction of CXCR3 ligands (Asselin-Paturel et al., 2005). However, a better understanding of the function of type I IFNs in the LN and their contribution to DC function is required.

In this study, we report that LNMs initiate an inflammatory response that leads to the activation of $CD11b^+$ LNDCs through an interleukin-1α (IL-1α)-mediated process, which is essential for the elicitation of the humoral response against influenza vaccine.

RESULTS

Influenza Vaccination Induces LN Macrophage Activation and Promotes Cell Death

To examine macrophage responses to UV-inactivated influenza virus vaccine (UV-PR8) in the popliteal LN, we employed different imaging techniques, including two-photon (2PM), electron microscopy (EM), and confocal microscopy. Three-dimensional (3D) reconstructions from 2PM images of the popliteal LN cortical area (Figure 1A) showed a significant decrease in the number of SSMs at 12 and 48 hr post-vaccination (p.v.) (Figure 1B). Additionally, the percentage of SSMs and MMs was reduced over time, whereas the percentage of DCs increased significantly (Figure 1C).

To further investigate the type of SSM death, we used in vivo staining with propidium iodide (PI) followed by 2PM imaging of LNs explanted at 4 hr p.v. (Figure 1D). 3D reconstruction analysis revealed a clear increase of PI+ SSMs in vaccinated groups compared to PBS-treated controls (Figure 1E), highlighting further the necrotic nature of SSM disappearance. To better examine the morphological features of the dying cells, EM was performed at 2 hr p.v., which revealed signs of necrosis in both SSMs (Figure 1F) and MMs (Figure 1G), including loss of plasma membrane integrity, mitochondria swelling, and chromatin condensation. Multiple endosomes containing viral particles were also detected in the cytoplasm of the observed cells, demonstrating their active phagocytic nature. To confirm SSM disappearance in vivo, we performed intravital 2PM on LysMCre-GFP mice. We observed that SSMs (sessile and large) that internalized UV-PR8 underwent cellular death, as evidenced by the loss of fluorescence, which is associated with the disruption of the plasma membrane. Moreover, dying SSMs did not form any blebs that are typically present in apoptotic cells (Figure 1H; Movie S1).

Using multicolor flow cytometric analysis, we assessed LN macrophage numbers in response to vaccination. A full description of the applied gating strategy is provided in Figure S1A. We found that the numbers of both SSMs and MMs were reduced by UV-PR8 administration by 12 hr p.v. (Figure 2A). We also observed that SSMs and MMs became rapidly activated following vaccine administration, as measured by the prominent upregulation of the early activation marker CD69 (Figures 2B and 2C, respectively; Figure S1B). Importantly, we observed that LNMs disappeared within the first 3 hr p.v. (Figures 2D and 2E) and remained absent for at least 1 week in the case of SSMs (Figure 1F) and 3 days in the case of MMs (Figure 1G).

The observed death mechanism was not exclusively associated with viral antigen, as SSM and MM numbers were also significantly reduced after vaccination with heat-inactivated *Streptococcus pneumoniae* (Figures S1C and S1D).

SSM Disappearance Is Dependent on Viral Internalization, TLR7 Recognition, and MyD88 Signaling, while MM Death Is Not

Having observed LNM disappearance, it was of interest to identify the factors involved in this phenomenon. To evaluate the role of viral entry in the observed death mechanism, we pretreated mice with two different anti-influenza antibodies: the neutralizing antibody H36-7 that binds specifically to the globular head of the viral hemagglutinin (HA) molecule of the PR8 H1N1 strain, thus preventing its interaction with the sialic acid (SA) of the target cell and blocking viral entry (Staudt and Gerhard, 1983), and

Figure 1. LN Macrophages undergo Necrosis-like Death after Influenza Vaccination

(A) The top panels show representative 3D reconstructions from 2PM images of popliteal LN from UV-PR8-administered CX3CR1-GFP reporter mice (green) at 12 and 48 hr p.v. (middle and right panels, respectively) following in vivo staining with anti-CD169-PE and anti-CD21/35-PB antibodies. The left panels show the unvaccinated control. The bottom panels present cross sections from the corresponding 3D reconstructions in the top panels. SSMs are indicated in yellow.

(B) Quantitative analysis of 2PM data showing SSM disappearance ($n \geq 5$ LNs).

(C) Changes in the percentages of SSMs ($CD169^+$, $CX3CR1^+$), MMs ($CD169^+$, $CX3CR1^-$), and DCs ($CD169^-$, $CX3CR1^+$) in the LN at 12 and 24 hr p.v. ($n \geq 4$ LNs).

(D) Representative 3D reconstruction from 2PM images of LN from CX3CR1-GFP reporter mice at 4 hr p.v. LNs were stained in vivo with anti-CD169-PB antibody and PI.

(E) Quantitative analysis of 2PM from LN follicular areas showing the increase in number of PI+ $CD169^+$ macrophages in the subcapsular sinus at 4 hr p.v. ($n \geq 10$ follicles).

(F and G) Representative electron micrograph of a SSM (F) and MM (G) at 2 hr p.v. In both cases, clear signs of necrosis, including loss of plasma membrane integrity (blue arrow), mitochondria swelling (green arrow), and multiple phagocytic vesicles with virus (red arrow, with higher magnification in the right panel), are evident.

(H) Intravital 2PM sequence from LysMCre-GFP reporter mice (green) showing SSM disappearance at 12 hr p.v. with DiI-labeled UV-PR8 (red) (Movie S1). Med, medullary area; Sub. S, subcapsular sinus area; Fo, follicle; MM, medullary macrophage; DC, dendritic cell.

In all figures, the presented data are representative of at least three independent experiments ($n \geq 3$). *$p < 0.1$; **$p < 0.01$; ***$p < 0.001$. Error bars, SD.

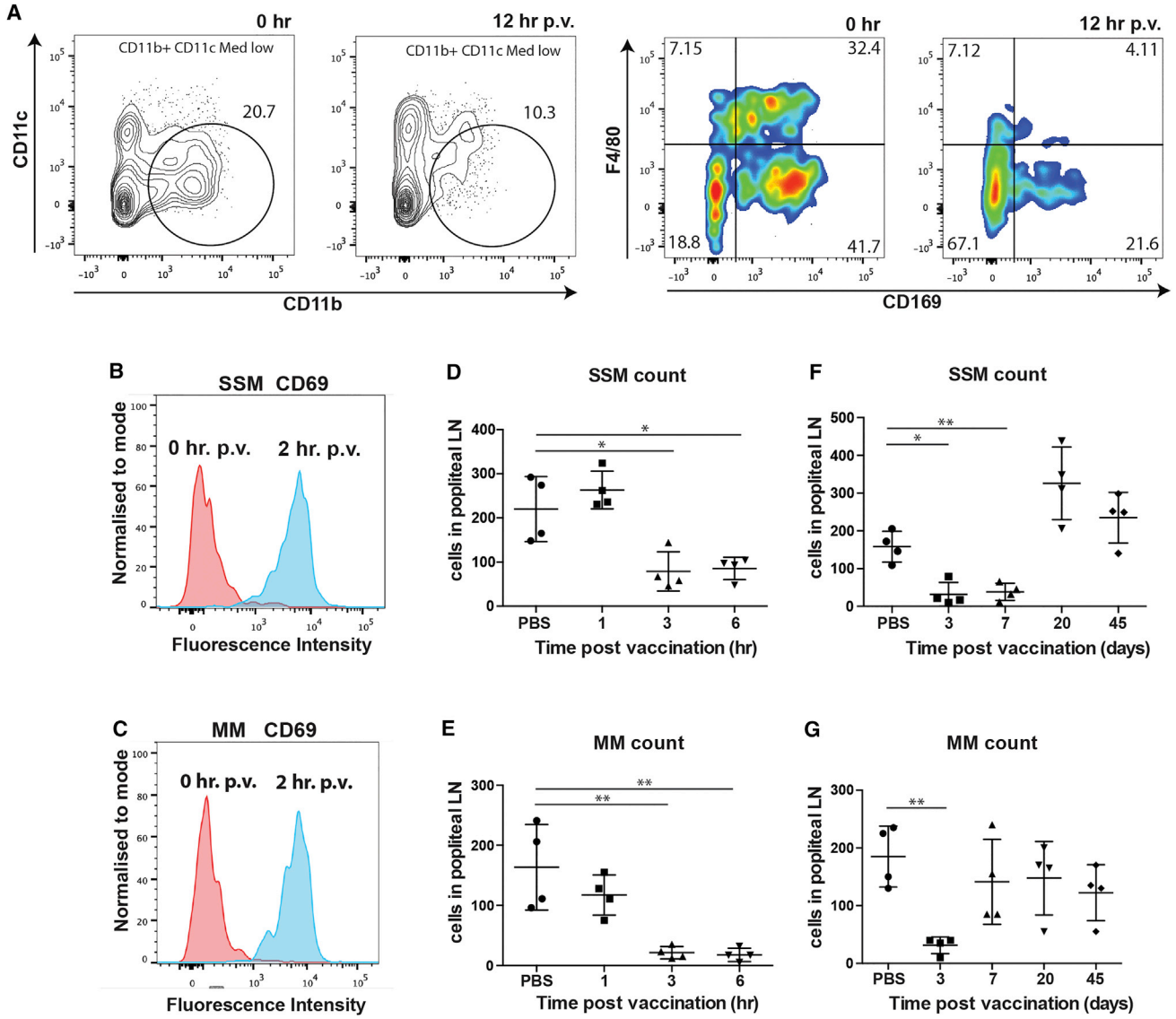

Figure 2. LN Macrophages Get Rapidly Activated and Are Absent from the LN during the First 3 Days p.v.

(A) Representative scatterplots from flow cytometric analysis of popliteal LNs showing an evident reduction of SSMs defined as CD3(−)/B220(−)/Ly6G(−)/Ly6C(−)/CD11c(inter./low)/CD11b(high)/MHCII(+)/F4/80(−)/CD169(+) in the popliteal LN at 12 hr p.v.

(B) Representative histogram of fluorescence intensity indicating differences in surface expression of the early activation marker CD69 in SSMs and MMs (C) at 2 hr. p.v. (blue) in comparison with the PBS-injected group (red).

(D–G) Flow cytometric analysis showing the rapid disappearance of SSMs (D) and MMs (E) following vaccine administration (10^5 PFU/footpad) and their reappearance at day 20 and day 7 p.v., respectively (F and G).

In all figures, the presented data are representative of at least three independent experiments ($n \geq 3$). *$p < 0.1$; **$p < 0.01$; ***$p < 0.001$. Error bars, SD.

the anti-fusion antibody FI6 that binds to the stem of the HA molecule, preventing the fusion of the virus with the endosome (Corti et al., 2011). Strikingly, immunization with H36-7 effectively prevented p.v. SSM death, while pretreatment with FI6 did not (Figure 3A), confirming that the SA-HA interaction and subsequent viral internalization is required for SSM death to be induced. In contrast, MM death was not prevented by H36-7 (Figure 3B), suggesting that virus internalization is not required for MMs to disappear. Moreover, SSM and MM disappearance was dependent on vaccine dosage, with complete depletion being induced with 10^5 plaque-forming units (PFUs) per footpad (Figures 3C and 3D). In an attempt to induce inflammation without the presence of virus, we administered alum, an adjuvant known for its proinflammatory properties. We observed that alum alone led to a significant reduction in the number of MMs (Figure S2G), while the number of SSMs remained unaffected (Figure S2F).

A previous study suggested that following parasitic infection, SSMs disappeared due to infiltrated neutrophils (Chtanova

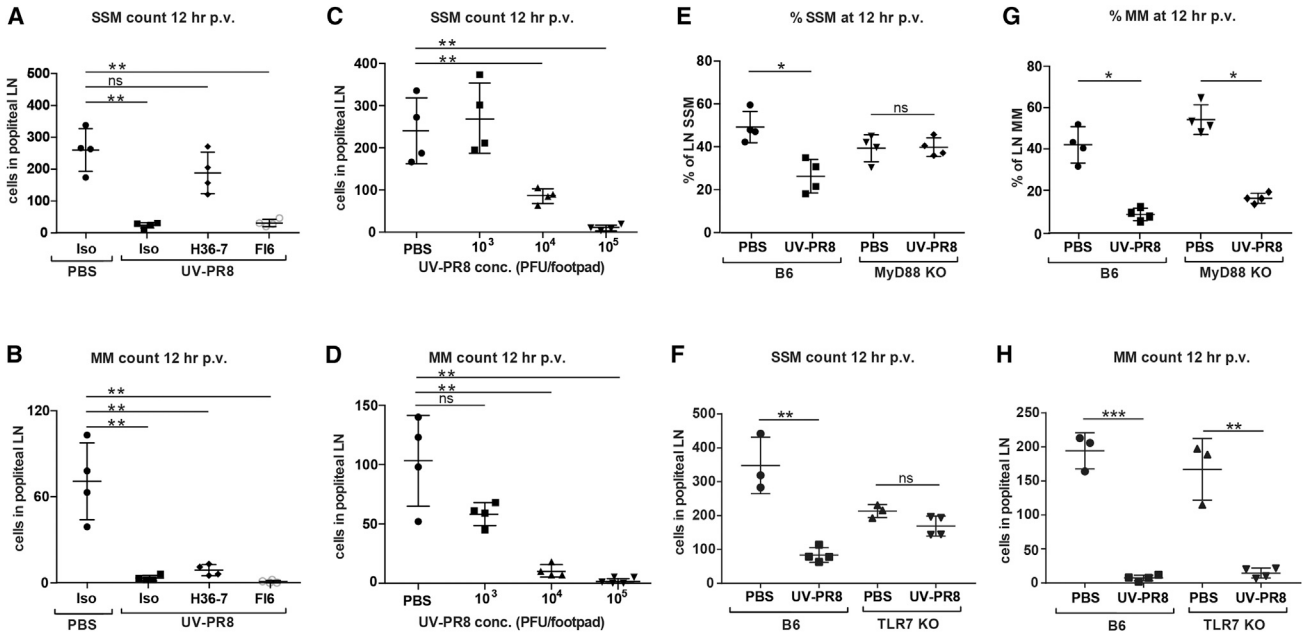

Figure 3. SSM Disappearance Requires Viral Internalization and Is Dependent on MyD88 and TLR7 Recognition, while MM Does Not

(A and B) Flow cytometric analysis of SSMs (A) and MMs (B) from mice passively immunized with the influenza-neutralizing antibody H36-7 and the anti-fusion antibody FI6 prior to the administration of UV-inactivated vaccine (UV-PR8). Pre-administration of H36-7 rescues SSMs from death following the administration of UV-PR8, but not MMs (A and B, respectively).

(C and D) Flow cytometric analysis showing a correlation between the number of SSMs (C) and MMs (D) and influenza vaccine dosage.

(E–H) Flow cytometric analysis of SSMs from MyD88 KO (E) and TLR7 KO (F) mice at 12 hr after administration of UV-PR8 showing that MyD88 and TLR7 are involved in the intracellular signaling events that lead to SSM death in response to UV-PR8, but not MM death (G and H).

In all figures, the presented data are representative of at least three independent experiments ($n \geq 3$). *$p < 0.1$; **$p < 0.01$; ***$p < 0.001$. Error bars, SD.

et al., 2008). In our work, we also observed recruitment of natural killer (NK) cells and neutrophils to the subcapsular sinus (data not shown). However, when these cells were eliminated using αNK1.1 and αLy-6G antibodies, respectively, we found that LNM disappearance remained unaffected (Figures S2C and S2D). A possible role of migratory DCs in the disruption of the SSM layer has been reported previously (Gaya et al., 2015). We found that migratory DCs did not contribute to the observed phenotype, as vaccinated CCR7 knockout (KO) mice, which are deficient in DC recruitment to the LN (Martín-Fontecha et al., 2003), exhibited the same SSM response as B6 mice (Figure S2E).

To determine the role of the inflammasome in this process, we vaccinated mice deficient in IL-1R, IL-1β, the adaptor protein ASC (apoptosis-associated speck-like protein with a CARD domain), or ICE (IL-1β-converting enzyme) and assessed their SSM numbers by flow cytometry at 12 hr p.v. Contrary to a recent report that described an inflammasome-dependent SSM burst in response to vaccinia virus (Sagoo et al., 2016), we observed a consistent decrease in SSMs in all of the tested KO strains p.v., confirming that, at least in our model, the inflammasome was not involved in LNM death (Figure S2A). In support of these results, we were not able to detect any upregulation of the transcripts of IL-1β or IL-18 during the first 24 hr p.v. (Figure S2B). In contrast, p.v. SSM disappearance was prevented in MyD88 KO mice (Figure 3E) and in Toll-like receptor 7 (TLR7) KO (Figure 3F), which confirmed that the death mechanism is dependent on viral recognition mediated by TLR7 signaling. However, MM death was not prevented in MyD88 KO (Figure 3G) or TLR7 KO (Figure 3H) mice, which suggests that death is triggered by different pathways in these cell populations.

LN Macrophages Initiate the Inflammatory Cascade that Follows Vaccine Administration

To evaluate the role that LNMs have on the initiation of the inflammatory response, we focused on the expression of different proinflammatory molecules after vaccination. Among the tested cytokines, we detected a rapid and significant secretion of IL-1α and IFN-β in the LN within the first 90 min p.v. (Figure 4A). To evaluate the duration and magnitude of the inflammatory reaction, we examined the levels of additional inflammatory molecules in the first 24 hr p.v. We observed a significant peak in the secretion of MIG, IP-10, KC, MCP-1, MIP-1α, and MIP-1β at 12 hr, followed by an abrupt decrease by 24 hr p.v. (Figure 4B).

To investigate the role of macrophage death in the induction of the inflammatory response, we measured the levels of secreted IFN-β and IL-1α in mice in which LN macrophages had been depleted with clodronate liposomes (CLLs) prior to vaccination. We observed that p.v. IFN-β secretion, which we found to be MyD88 independent, was abolished in CLL-pretreated mice (Figure 4C, left). Similarly, secretion of IL-1α was inhibited in

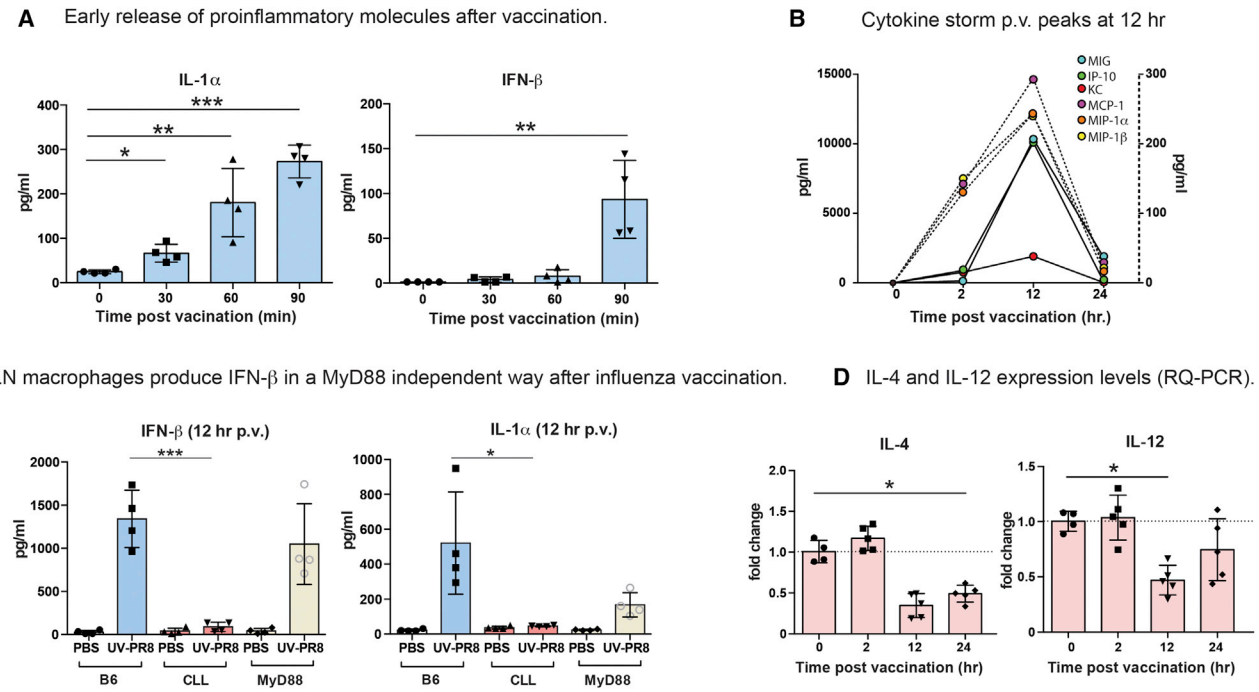

Figure 4. LNMs Are Responsible of the Initial Type I IFN Response that Follows Vaccination

(A) Secretion of the proinflammatory cytokines IL-1α and IFN-β in the first 90 min p.v. Cytokine levels were measured in LN exudates by a cytoplex assay.

(B) Levels of acute-phase cytokines MIG, IP-10, KC, MCP-1, MIP-1α, and MIP-1β in the LN in the first 24 hr p.v. A peak of secretion was measured at 12 hr p.v. Dotted lines refer to the right-hand axis.

(C) Levels of secreted IFN-β and IL-1α in LNs from macrophage-depleted (CLL-pretreated) and MyD88 KO mice at 12 hr p.v. The expression of these cytokines requires the existence of macrophage prior to vaccination.

(D) RNA expression levels of the cytokines IL-4 and IL-12 during the first 24 hr that follows vaccination.

In all figures, the presented data are representative of at least three independent experiments ($n \geq 3$). *$p < 0.1$; **$p < 0.01$; ***$p < 0.001$. Error bars, SD.

this group, although the production of this cytokine was dependent on MyD88 (Figure 4C, right). Moreover, mRNA levels of the cytokines IL-4 and IL-12, which are important for the differentiation of naive T cells into Th2 and Th1, respectively, were found to be significantly downregulated at 12 hr p.v. (Figure 4D). Taken together, these findings suggest that, upon vaccine challenge, macrophages are key to the production of inflammatory cytokines in the draining LNs.

IFN-β Produced by MMs Triggers the IL-1α Inflammatory Cascade

To investigate whether macrophages were the source of the type I IFN response, we performed intracellular staining of IFN-β at 2 hr p.v. Moreover, since DCs had been previously identified as a source of IFN-β in the LN (Iannacone et al., 2010), it was of interest to include them in our investigation. Flow cytometric analysis showed that both macrophages and DC produced IFN-β, but to a different extent. Although the IFN-β+ cell count was similar for both LNMs and DCs, at 2 hr p.v. (data not shown), the former expressed IFN-β at levels ~1,000 times higher than the latter (Figure 5A, left). Interestingly, a more detailed characterization of the macrophage subtype showed that at 2 hr p.v., the majority of IFN-β+ macrophages were MMs (Figure 5B). These results were further confirmed by immunohistochemical analysis in which we observed a prominent expression of IFN-β that was associated with $CD169^+$ MMs located in the interfollicular and medullary areas at 2 hr p.v. (Figure 5C), compared to controls (Figure S3A). Additionally, IFN-β expression appeared to be induced in a positive feedback loop initiated by macrophages, as IF-α/β receptor (IFNAR) KO or macrophage-depleted (CD169DTR) mice presented significantly lower IFN-β levels than B6 controls at 12 hr p.v. (Figure 5D).

To study the mechanism of action of IL-1α and IFN-β, we examined the effect of different concentrations of their recombinant forms alone (without vaccination with UV-PR8). At 12 hr post-administration (footpad injection) of recombinant IL-1α or recombinant IFN-β, we measured concentrations of inflammatory cytokines in the LN similar to the ones previously detected following vaccination. Interestingly, IFN-β was sufficient to induce secretion of IL-1α, albeit at levels inversely proportional to the administered dose. Strikingly, both IL-1α and IFN-β were sufficient to induce the expression of the chemoattractant protein MCP-1 that is involved in the trafficking of monocytes and DCs (Figure 5E).

To examine the involvement of LNMs in the expression of IL-1α, immunostaining was performed in LN sections at 2 hr p.v., and results confirmed that LN macrophages act as producers of this cytokine (Figure 5F). Additionally, intracellular

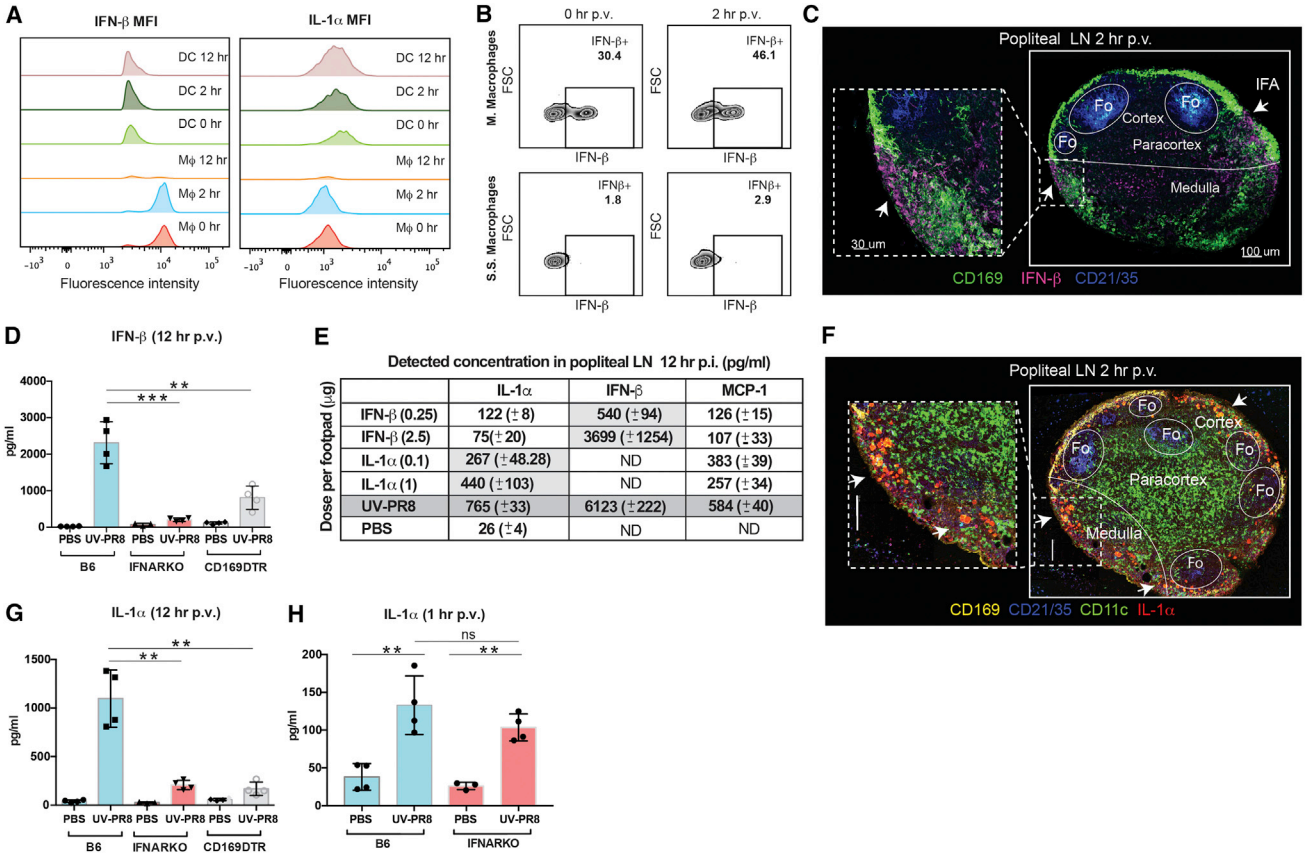

Figure 5. IFN-β Produced by MM Induces the Expression of IL-1α after Vaccination

(A) Representative results showing intracellular quantification of IFN-β (left) and IL-1α (right) in LNMs (gating strategy described in Figure 1) and DCs ($CD3^-/CD11c^{high}/CD169^-$) at 0, 2, and 12 hr p.v. Histograms represent fluorescence intensity that indicates the level of expression of each of the cytokines in the examined cells.

(B) Representative plots showing intracellular quantification of IFN-β in MM (up) and SSM (down) at 2 hr p.v.

(C) Confocal micrographs showing expression of IFN-β (purple) in the medullary and interfollicular areas of the LN associated with MMs ($CD169^+$; green) at 2 hr p.v.

(D) Levels of IFN-β in LNs from B6, IFNAR KO, and macrophage-depleted (CD169-DTR) mice at 12 hr p.v.

(E) Detected IL-1α, IFN-β, and MCP-1 levels in the popliteal LN after administration of two concentrations of recombinant IFN-β or IL-1α alone (without UV-PR8) compared to controls (UV-PR8 or PBS treatments). SD is indicated in brackets; ND indicates non-detectable amounts.

(F) Confocal micrographs showing the expression of IL-1α (red) at 2 hr p.v. associated to LN macrophages ($CD169^+$; yellow) in the cortical and medullary area of a popliteal LN. The follicular area was stained with anti-CD21/35-PB antibody (blue).

(G and H) Levels of IL-1α in LN from B6, IFNAR KO, and macrophage-depleted (CD169-DTR) mice at 12 hr p.v (G) and at 1 hr p.v (H).

In all figures, the presented data are representative of at least three independent experiments ($n \geq 3$). *$p < 0.1$; **$p < 0.01$; ***$p < 0.001$. Error bars, SD.

staining of IL-1α confirmed that both LNMs and DCs are able to produce this potent cytokine at 2 hr p.v. (Figure 5A, right). Importantly, IL-1α expression appeared to be dependent on signaling through the type I IFN receptor at 12 hr p.v., as IFNAR KO mice showed significantly lower levels than B6 controls (Figure 5G). However, the expression of IL-1α at 1 hr p.v. was similar in B6 and IFNAR KO mice, which suggests an IFN-independent mechanism in the initial release of this cytokine (Figure 5H).

LNMs Induce the Activation and Migration of LNDCs and Influence Their Capacity to Present Antigen

Having established the necrotic nature of LNM death and their response after vaccine administration, we hypothesized that the release of inflammatory molecules may mediate the activation of LNDCs. To investigate a possible link between LNM death and LNDC migratory dynamics, we performed 2PM 3D reconstruction analysis on CD11c-YFP mice at 12 hr p.v., which revealed an attraction of $CD11c^+$ DCs toward the areas where LNMs were present (Figure 6A). The analysis of these data demonstrated a clear decrease in the distance between LNDCs (mainly located in the paracortex in non-vaccinated animals) and the LNM layer (Figure 6B). To investigate the effect of macrophage-mediated antigen capture by DCs on their capacity to stimulate CD4 T cells, we isolated DCs from CLL-pretreated and control mice at 12 hr p.v., co-cultured them in vitro with HA-specific $CD4^+$ T cells, and measured the division index

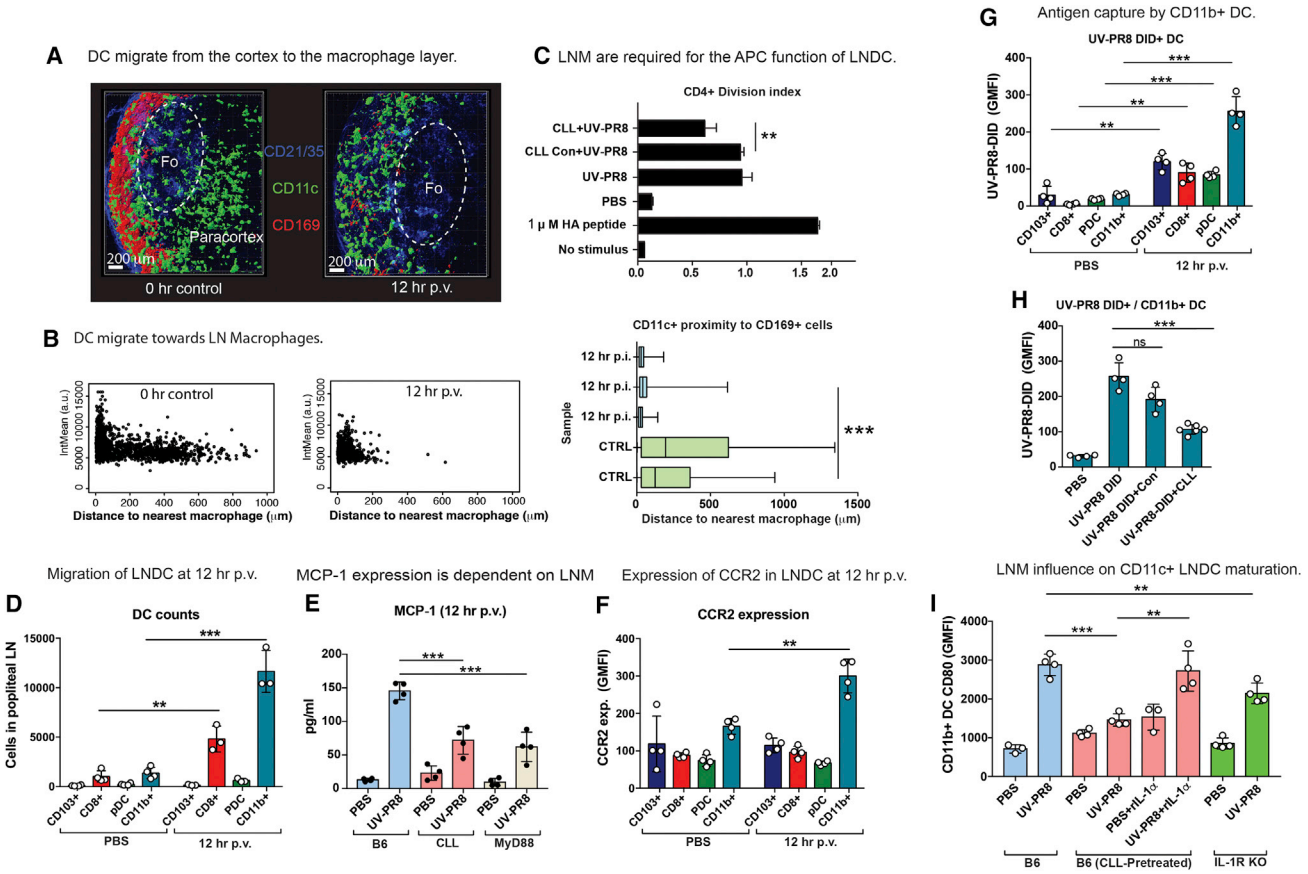

Figure 6. LNMs Induce the Activation, Migration, and Antigen Presentation Capacity of CD11b$^+$ LNDCs

(A) Representative 2PM showing the position of CD11c-YFP$^+$ cells in a control (left) or vaccinated mouse with respect to the LNM layer (red) at 12 hr p.v.

(B) Representative dot plot of the distance between LNDCs and the nearest macrophage (µm) at 12 hr in control (left) and vaccinated (middle) mice. The y axis represents mean intensity expressed in arbitrary units (a.u.). Right: chart showing the CD11c$^+$ cells in relation to CD169$^+$ LNMs.

(C) Flow cytometric assessment of the division index of transgenic influenza HA-specific CD4$^+$ T cells after being cocultured for 72 hr with DCs isolated from mice that had received one of the following treatments: CLL or control liposomes followed by vaccination, vaccine alone, PBS, HA peptide, or no stimulus. DCs were isolated at 12 hr p.v. (left).

(D) Flow cytometry data showing the number cells in four different DC subpopulations (CD103$^+$, CD8$^+$, pDCs, and CD11b$^+$ DCs) present in the LN at 12 hr p.v.

(E) Levels of secreted MCP-1 in LNs from macrophage-depleted (CLL-treated) and MyD88 KO mice at 12 hr p.v.

(F) Flow cytometry data showing expression levels of CCR2 in LNDCs at 12 hr p.v.

(G) Flow cytometry data showing changes in the GMFI of the different DC subpopulations that have captured DiD-labeled UV-PR8.

(H) Differences in virus uptake in CD11b$^+$ DCs from mice that were administered PBS or UV-PR8-DiD and test groups that were pretreated with clodronate (CLL)- or PBS-containing liposomes (control liposomes).

(I) GMFI analysis showing differences in surface expression of the costimulatory molecule CD80 at 12 hr p.v. in DCs from vaccinated or PBS-injected mice that had been pretreated with CLL and coadministered with recombinant IL-1α. Mice deficient in IL-1 receptor were also tested (right).

In all figures, the presented data are representative of at least three independent experiments ($n \geq 3$). *$p < 0.1$; **$p < 0.01$; ***$p < 0.001$. Error bars, SD.

of the latter. We found that DCs from macrophage-depleted mice had a significantly impaired ability to stimulate CD4$^+$ T cells, compared to control treatments (Figure 6C), confirming the requirement of the LNM-DC interaction for effective DC function.

To study the effect of macrophage-induced inflammation on LNDCs, we evaluated antigen capture and maturation in four groups of DCs divided according to their expression of specific surface markers (Merad et al., 2013) (Figure S4A). We confirmed that the presence of migratory CD103$^+$ DCs and plasmocytoid dendritic cells (pDCs) was negligible in the draining LN at 12 hr p.v. Interestingly, we also observed a significant increase in the number of CD8$^+$ DCs and CD11b$^+$ DCs at this time point (Figure 6D).

To understand the signals that directed the movement of these cells, and considering that the type I IFN response initiated by LNMs induced the release of MCP-1 (Figures 5E and 6E), we analyzed the expression of its receptor, CCR2, in the different DC subtypes. Interestingly, we observed a significant increase in the number of CD11b$^+$ DCs that expressed CCR2 (data not shown) and a prominent upregulation of the expression of this receptor in these cells at 12 hr p.v. (Figures 6F and S4B).

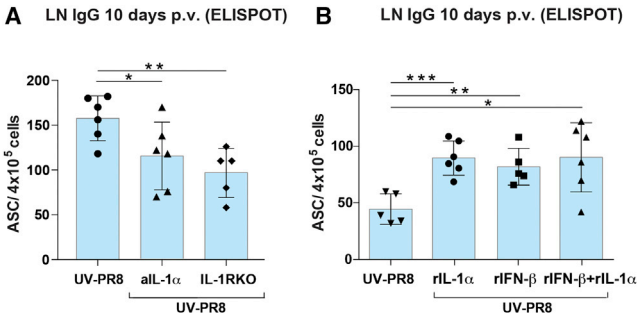

Figure 7. The Inflammation Initiated by LNMs Is Essential for the Development of an Effective B Cell Response

(A) Number of influenza-specific IgG ASC in LNs from mice pretreated with anti-IL-1α compared with a control group vaccinated with UV-PR8 alone or deficient in the IL-1 receptor (IL-1RKO). LNs were collected at 10 days p.v.

(B) Number of influenza-specific IgG ASC in LNs from mice pretreated with rIL-1α, rIFN-β, or a combination of these cytokines compared with a control group vaccinated with UV-PR8 alone. LNs were collected at 10 days p.v.

In all figures, the presented data are representative of at least three independent experiments ($n \geq 3$). *$p < 0.1$; **$p < 0.01$; ***$p < 0.001$. Error bars, SD.

We also observed clear differences in the capacity of the different DC populations to capture virus, the CD11b$^+$ DC subset being associated with the highest uptake of the vaccine (Figure 6G). Moreover, we found that the amount of labeled UV-PR8 captured by CD11b$^+$ DCs in macrophage-ablated mice decreased compared to the empty liposomes or the untreated groups, as shown by geometric mean fluorescence intensity (GMFI) analysis (Figure 6H). This observation reflected either the reduction in retained quantity and availability of antigen in the LN (Gonzalez et al., 2010) due to macrophage depletion or the reduced ability of DCs to capture antigen because of the lack of macrophage-induced inflammatory signals.

Moreover, at 12 hr p.v., the expression of the costimulatory molecules CD80 and CD86 was significantly lower in CD11b$^+$ DCs from CLL-pretreated mice than in the untreated group (Figures 6I and S4C, respectively). Interestingly, co-administration of IL-1α and vaccine restored CD80 expression in CLL-pretreated mice to the same level as in mice administered UV-PR8 alone. We also confirmed that CD80 expression by CD11b$^+$ DCs was lower in vaccinated IL-1R KO mice than in the equivalent B6 controls (Figure 6I).

The Inflammatory Cascade Associated with IL-1α Release Is Essential for Humoral Immunity in the Draining LN

As mentioned previously, LN macrophages play a critical role in the initiation of the inflammatory response. Therefore, to study the effect that macrophage-dependent inflammation has on antibody production, we performed a series of immunizations in mice treated with anti-IL-1α antibody and in mice deficient in IL-1R. We observed that at 10 days p.v., the number of influenza-specific ASC in the draining LN was significantly reduced compared to the control mice in all of the tested groups, which highlighted that macrophage-dependent IL-1α-mediated inflammation is required for the development of an effective B cell response in this organ (Figure 7A). Moreover, to determine whether IL-1α and IFN-β have an adjuvant action, mice were immunized with the influenza vaccine alone or vaccine supplemented with recombinant IL-1α, IFN-β, or both. Strikingly, at 10 days p.v. the number of ASC were significantly increased in the groups treated with the recombinant IL-1α and IFN-β in comparison with mice treated with the vaccine alone (Figure 7B).

DISCUSSION

Since the identification of macrophage death as an immunological reaction (Barth et al., 1995), it has become apparent that this phenomenon involves the interplay of signaling cascades triggered by the presence of antigen. However, it is only recently that studies have focused on SSM rupture as an event that mobilizes innate and adaptive immunity (Gaya et al., 2015; Staudt and Gerhard, 1983).

We observed that following UV-PR8 administration, both SSMs and MMs undergo necrotic death through a process that is dependent on vaccine dosage. The mechanism we describe differs from the one presented in previous studies. Gaya and colleagues (Gaya et al., 2015) reported that SSM disappearance was dependent on the infiltration of migratory DCs. However, in our observations, infiltrated DCs did not contribute to the described phenotype, as CCR7 KO mice that are deficient in DC recruitment to the LN showed the same SSM response as mice in the B6 control group. Moreover, we observed that SSM death occurs within the first 3 hr after vaccination, much earlier than the time required for DCs to migrate to the LN (Martín-Fontecha et al., 2003), and we could not observe any recruitment of migratory DCs expressing CD103 in the LN at 12 hr p.v. Furthermore, Gerner and colleagues (Gerner et al., 2015) questioned the paradigm that T cell induction is exclusively mediated by DCs migrating from the peripheral organs, as these cells require extended periods of time to reach the draining LN. We also discarded the possibility that LNM death is affected by infiltrated innate immune cells, as depletion of NK cells or neutrophils did not prevent macrophage disappearance. Interestingly, Sagoo and colleagues (Sagoo et al., 2016) described a mechanism by which SSMs undergo inflammasome-mediated pyroptosis after administration of live vaccinia virus. In our model, although UV-irradiated influenza virus retained its ability to enter the host cell, we eliminated the possible involvement of the inflammasome pathway, given that depletion of molecules associated with this pathway did not prevent SSM death.

Importantly, pretreatment with an antibody against the SA binding site of PR8 HA prevented SSM death, while pretreatment with the FI6 antibody that binds to the fusion domain of HA did not, indicating that influenza viral entry via the HA-SA interaction is required to trigger this mechanism. Once inside the cell, the single-stranded viral RNA is recognized by TLR7 and triggers SSM death in a process that is dependent of the adaptor protein MyD88. Interestingly, Gaya and colleagues recently described a mechanism in which MyD88 was also involved in SSM death following infection (Gaya et al., 2015).

Previous studies have proposed a model in which SSMs capture and shuttle intact antigen from the subcapsular sinus to

B cells in the underlying follicle (Carrasco and Batista, 2007; Junt et al., 2007). We observed that elimination of SSMs as a consequence of antigen administration occurs soon after vaccination, and SSMs remain absent for at least 1 week thereafter (Figure 2F). Therefore, it is unlikely that these cells could play a role as APCs. However, it could be possible that MMs, which reappear within the first 7 days p.v. (Figure 2G), might be involved in antigen presentation, a possibility that requires further investigation.

We propose an alternative scenario in which the contribution of LNMs to the adaptive response is associated with their role in the initiation of the inflammatory response that follows vaccination. This process is initiated by the secretion of IFN-β, which we found to be dependent on the presence of macrophages. These results are in agreement with previous reports that demonstrated an important role for macrophage-produced type I IFN in different immunological processes such as the T central memory response against virus (Sung et al., 2012) or the migration of pDCs from the deep cortex to the SCS area following viral infection (Asselin-Paturel et al., 2005; Iannacone et al., 2010). However, in this work, we demonstrated that MMs, but not SSMs, are the cells principally responsible for IFN-β secretion. This suggests that the interfollicular regions in the subcapsular sinus and the medullary part of the LN might be the most relevant areas in which cell activation and antigen presentation occur.

Type I IFNs are known to be secreted in response to UV-inactivated influenza virus in a process that is dependent on MyD88 (Diebold et al., 2004), an adaptor protein that plays a key role in the defense of the host against many pathogens (Seo et al., 2010). The role of type I IFN is to induce an antiviral state through the production of proinflammatory cytokines and instruct the adaptive immune response against the virus (Iwasaki and Pillai, 2014). Macrophage activation following recognition of virus by TLR results in the expression of nuclear factor κB (NF-κB)-mediated proinflammatory cytokines or the production of IRF7-mediated type I IFN (Iwasaki and Pillai, 2014; Malmgaard et al., 2004). Surprisingly, we found that vaccine-induced IFN-β production was MyD88-independent. This result was in contrast to the role of TLR7 in the induction of IFN-β and suggested an alternative mechanism that may involve other sensing molecules such as RIG-I, a previously described type I IFN inducer in infected and immune cells (Kato et al., 2005). However, we found that TLR7 recognition and MyD88 signaling were important for the induction of IL-1α and MCP-1 in a process mediated by the recognition of influenza single-stranded RNA in the endosomal compartment of LNMs and DCs. We observed that MMs located in the interfollicular area (IFA) and medullary area of the LN were the cell type responsible for initial IFN-β secretion. From their position in the IFA, these cells could generate an IFN gradient that might contribute to the activation of nearby SSMs. Moreover, the administration of recombinant IFN-β alone was sufficient to induce secretion of IL-1α. In addition, IL-1α production was impaired in mice deficient in IFNAR or in mice in which macrophages had been ablated at 12 hr p.v., confirming the role of IFN-β in the observed peak in IL-1α secretion.

Our model agrees with the ''inflammatory loop'' model described by Di Paolo and Shayakhmetov (Di Paolo and Shayakhmetov, 2016) in which inflammation is initiated by stressed or damage cells via IL-1α-dependent activation of chemokines that recruit inflammatory cells to the site of infection. Interestingly, previous reports have stressed the role of prestored IL-1α as an alarmin molecule involved in the initiation of the inflammatory response in the context of sterile inflammation (Rider et al., 2011) or other physiological stimuli (Di Paolo and Shayakhmetov, 2016). To act as an extracellular alarmin, pro-IL-1α requires the loss of plasma membrane integrity, which is indicative of necrotic cell death (Galluzzi et al., 2015). In this work, we confirmed by EM the loss of plasma membrane integrity in the LNM following influenza vaccination (Figures 1F and 1G). In addition, we observed that LNMs express substantial amounts of IL-1α at steady state (Figure S3B). Interestingly, we observed that the initial release of IL-1α was independent of the type I IF signal. Thus, it might be hypothesized that the early levels of this cytokine measured in the LN are associated with the necrotic death of macrophages, which constitutively express and store IL-1α, as confirmed by immunohistochemistry and fluorescence-activated cell sorting (FACS) studies. However, the observed peak in expression of IL-1α at 12 hr p.v. is most likely due to de novo synthesis by LNDCs, triggered by the disappearance of the LNM.

The observations in our model agree with previous studies that describe the leakage of cytosolic IL-1α to the surrounding milieu as a result of cell death caused by injury or infection (Chen et al., 2007; Eigenbrod et al., 2008). Regarding the source of IL-1α in the LN, although LNMs and DCs appeared to be the major producers of this cytokine, we could not discard the contribution of other myeloid or stromal cells. Similarly, we could not rule out the possibility that alternative mechanisms other those that involve IL-1α might affect the activation of DCs in vivo. Additionally, the direct effect of IL-1α on LNDCs needs to be further evaluated.

In this work, we showed that the type I IFN reaction, initiated by LNMs, promotes B cell responses to influenza vaccine in the LN, given that transient treatment with an antibody against IL-1α reduced immunoglobulin G (IgG) production significantly. Additionally, co-administration of vaccine and recombinant IL-1α increased the humoral response in the draining LN. Our results are in agreement with other studies that suggest that IL-1α and IL-1β serve as mucosal adjuvants when administered with soluble protein antigens (Staats and Ennis, 1999).

Different studies have recently demonstrated the capacity of DCs to relocate to the LN interfollicular areas in which antigen is captured (Iannacone et al., 2010; Woodruff et al., 2014). However, the specific effect of the IL-1 inflammatory pathway on DC activation in the LN is not fully understood. We observed that $CD11b^+$ DCs in the draining LN have a prominent role capturing influenza virus. Additionally, IL-1α and IFN-β, initially secreted by LNMs, contribute to the maturation of this DC subset based on the effect that these molecules have on the expression of the costimulatory markers CD80 and CD86. Importantly, IL-1α and IFN-β induced the expression of MCP-1 that attracts $CCR2^+$ $CD11b^+$ DCs to the areas in which antigen and DAMP from necrotic SSMs remain. Moreover, the presence of LNMs appeared to be necessary for antigen presentation between LNDCs and $CD4^+$ T cells, as demonstrated by the lower capacity

of DCs isolated from macrophage-depleted mice to present antigen to influenza-specific $CD4^+$ T cells.

In this study, we provide a link between LNM death in response to vaccination and the promotion of DC function in the LN through a mechanism that involves TLR7-mediated viral recognition and the release of IFN-β and the alarmin molecule IL-1α. These cytokines activate DCs and stimulate them to secrete IL-1α in a positive feedback loop. Importantly, secretion of MCP-1, which is also induced by the type I IFN response, attracts $CCR2^+$ $CD11b^+$ DCs to the areas with remaining antigen and DAMP from necrotic SSMs, ensuring effective DC activation and function.

Based on our results, we can consider the stimulation of the IL-1α inflammatory pathway as a possible strategy for the enhancement of APC function in LNDCs and the improvement of the humoral response against influenza vaccine.

EXPERIMENTAL PROCEDURES

Mice

Mice were bred in-house or acquired from Janvier Labs (C57BL/6) or Charles River Laboratories (BALB/c). The following transgenic strains were used: CX3CR1-EGFP (Jung et al., 2000), IL-1R/KO (Labow et al., 1997), IL-1β/KO (Matsuki et al., 2006), ASC/KO (Mariathasan et al., 2004), ICE/KO (Kuida et al., 1995), MyD88/KO (Hou et al., 2008), IFNAR KO (Müller et al., 1994), LysMcre-GFP (Clausen et al., 1999), TLR-7/KO (Lund et al., 2004), and influenza HA-specific CD4 T cell receptor α/β (TCR-α/β) (Kirberg et al., 1994). All strains had the C56BL/6 background except for the HA-specific CD4 TCR that was on BALB/c. Mice were maintained in specific-pathogen-free facilities at the Institute for Research in Biomedicine, Bellinzona. Experiments were performed in accordance with the Swiss Federal Veterinary Office guidelines, and animal protocols were approved by the veterinarian local authorities.

Antigen Administration and Injections

Influenza virus strain A/PR/8/34 was grown, purified, inactivated, and labeled as described previously (Gonzalez et al., 2010). Different concentrations of inactivated virus were injected into the footpad of anesthetized mice at different time points prior to LN collection. Virion dosage ranged from 10^3 to 10^5 PFUs per footpad in a final volume of 10 μL. For macrophage depletion, mice were injected in the footpad with 10 μL CLL or PBS-containing (control) liposomes (Clodronateliposomes.org) at days 5 and 3 prior to immunization. For NK cell and neutrophil depletion, 300 μg of the depletion antibodies αNK1.1 (clone PK136) and αLy-6G (clone 1A8) (BioXCell) were administered intraperitoneally (i.p.) and intravenously (i.v.) at days 3 and 1 before vaccine administration, respectively. Macrophage, NK cell, and neutrophil disappearance following depletion treatment was assessed by FACS (data not shown). For follicular dendritic cell (FDC) and SSM labeling, mice received 0.5 μg fluorescence-labeled αCD21/35 and αCD169 (BioLegend), respectively, which was injected into the footpad 3 to 5 hr prior to image acquisition. For cytokine blocking, the antibody αIL-1α (clone ALF-161, BioXCell) was administered i.v. at a dose of 200 μg/animal, as well as footpad at 61 μg/animal, at the time of vaccination. Recombinant cytokines were injected at indicated amounts into the footpad at the time of vaccination and 6 hr p.v., except for the ELISPOT experiment, in which only one injection of 0.1 μg rIL-1α, 0.25 μg of rIFN-β, or a combination of both was administered into the footpad 30 min p.v..

Flow Cytometry

Popliteal LNs were collected, disrupted with tweezers, and digested for 10 min at 37°C in an enzyme mix composed of DNase I (0.28 mg/mL, Amresco), dispase (1 U/mL, Corning), and collagenase P (0.5 mg/ml, Roche) in calcium- and magnesium-free PBS (PBS−) followed by a stop solution composed of 2 mM EDTA (Sigma-Aldrich) and 2% heat-inactivated filter-sterilized fetal calf serum (Thermo Fisher Scientific) in PBS− (Sigma-Aldrich). Fc receptors were blocked (αCD16/32, BioLegend) followed by surface staining and analyzed by flow cytometry on an LSRFortessa (BD Biosciences). Where indicated, intracellular staining was performed (88/8824/00, eBioscience) following the manufacturer's instructions. Data were analyzed using FlowJo software (TriStar), including the calculation of division index.

Immunohistology and Microscopy

Mice were anesthetized with a mixture of ketamine (100 mg/kg bodyweight, Parke Davis) and xylazine (10 mg/kg bodyweight, Bayer) and perfused with a fixative solution made of 10 mL of 0.05 M phosphate buffer containing 0.1 M L-lysine, 4% paraformaldehyde, and 2 mg/mL $NaIO_4$ at pH 7.4 (PLP). Popliteal LNs were subsequently collected and incubated in 30% sucrose phosphate-buffered solution overnight. Tissues were snap frozen in O.C.T. compound (VWR Chemicals Leuven). 10- to 30-μm sections were cut with a microtome, blocked with proper sera, and stained with the indicated antibodies (see antibody section). Immunofluorescence confocal microscopy was performed using a Leica TCS SP5 confocal microscope (Leica Microsystems). Micrographs were acquired in sequential scans and merged to obtain a multicolor image. Images were analyzed using Imaris software (Bitplane AG). Transmission electron microscopy was performed as described previously (Roozendaal et al., 2009).

In Vivo PI Staining

To quantify necrotic SSMs following vaccination, C57BL/6J mice were injected with 10 μL of 10^7 PFU/mL UV-PR8 into the footpad. 1 hr later, SSM and LN follicles were labeled by footpad administration of 0.25 μg of fluorescently labeled αCD169 and 0.5 μg of αCD21/35 antibodies (BioLegend). 3 hr later, 20 μg of PI (Sigma-Aldrich) was administered by footpad injection and LN were harvested immediately. 3D reconstructions of a complete follicular area and overlying SSM layer were made using two-photon intravital microscopy (150-μm tissue depth). Quantification of necrotic SSMs was performed using Imaris software based on CD169 expression, PI signal, sphericity, and volume.

Antibodies

In this study, the following antibodies (BioLegend) were used: αB220 (RA3-6B2), αCD4 (GK1.5), αCD21/35 (7E9), αF4/80 (BM8), αCD40 (3/23), αCD80 (16-10A1), αCD11c (N418), αCD169 (3D6.112), αCD3 (17A2), αNK1.1 (PK136), αCD11b (M1/70), αCD69 (H1.2F3), αI-A/I-E (M5/114.15.2), αLy-6G (1A8), αCD16/32 (93), αMHCI (SF1-1.1.1), αGr-1 (RB6-8C5), αCD86 (GL-1), αLy-6C (HK1.4), αIFN-β (PBL Assay Science), rabbit αIFN-β (Abcam), αIg(H+L)-AP, αIgG-biot, αIgM-biot (Southern Biotech), αCCR2 (R&D Systems), H36-7, FI6 (HUMABS BioMed), and depletion antibodies αIL6 (MP5-20F3), αIL-1α (ALF-161), and rat IgG1 isotype (HRPN) (all from BioXCell).

ELISPOT

Mice were immunized with different doses of UV-inactivated PR8 virus (10^3 to 10^5 PFU per footpad) subcutaneously. For enzyme-linked immunospot assay (ELISPOT), on day 10 p.v., popliteal LNs were removed aseptically, disrupted, and passed through a 40-μm cell strainer. 4×10^5 cells were plated on UV-PR8-coated (10^7 PFU/mL) filter plates ($MultiScreen_{HTS}$, Merck Millipore) and incubated for 16 hr at 37°C. For detection, a biotin-conjugated αIgG or αIgM was used, followed by streptavidin-conjugated horseradish peroxidase (HRP). A developing solution consisting of 200 μL 3-amino-9-ethylcarbazole (AEC) solution (Sigma) in 9 mL sodium acetate buffer containing 4 μL 30% H_2O_2 was subsequently added. Spots were read on a C.T.L. ELISPOT reader using ImmunoSpot 5.1 software (Cellular Technology).

In Vitro Evaluation of Hemagglutinin-Specific Transgenic $CD4^+$ T Cell Responses

LN-resident DCs were isolated by digestion as described previously (Gonzalez et al., 2010). Samples were enriched for $CD11c^+$ DCs by magnetic separation with microbeads (Miltenyi Biotech). Purity was evaluated by FACS and was always higher than 85%. LNs were collected from T cell antigen receptor

transgenic mice with expression of an αβ T cell antigen receptor specific for influenza HA peptide, and single-cell suspensions were prepared. Following lysis of red blood cells by ammonium chloride-potassium bicarbonate buffer (BioWhittaker, Lonza), cells were labeled for 10 min with 5 μM CFSE (Invitrogen) and washed thoroughly. HA-specific $CD4^+$ T cells (2×10^5) were cultured for 72 hr together with DCs (5×10^4). Proliferation was measured by flow cytometry and presented as division index.

Cytoplex Assay

LEGENDPlex assays (Mouse Proinflammatory Chemokine Panel and Mouse Inflammation Panel; BioLegend) were performed to monitor cytokine and chemokine expression. Briefly, popliteal LNs were collected and carefully disrupted in 100 μL ice-cold phosphate buffer, minimizing cell rupture. The suspension was centrifuged at 1,500 rpm for 5 min, and the supernatant was collected. 25 μL supernatant was used for the protocol following the manufacturer's instructions. Samples were analyzed by flow cytometry on an LSRFortessa (BD Biosciences), and data were analyzed using LEGENDPlex software (BioLegend).

qPCR

To measure the expression levels of the cytokines IL-1β, IL-12, IL-4, and IL-18 the following sets of primers were designed: *IL-1β* forward, 5′-TGTTTTCCTCCTTGCCTC-3′; *IL-1β* reverse, 5′-GCTGCCTAATGTCCCCTT-3′; *IL-12* forward, 5′-TGTGGAATGGCGTCTCTG-3′; *IL-12* reverse, 5′-CAGTTCAATGGGCAGGGT-3′; *IL-4* forward, 5′-GAGCTCGTCTGTAGGGCT-3′; *IL-4* reverse, 5′-CCGAAAGAGTCTCTGCAG-3′; *IL-18* forward, 5′-GGTTCCATGCTTTCTGGACT-3′; and *IL-18* reverse, 5′-GGCCAAGAGGAAGTGATTTG-3′. Popliteal LNs were collected at 0, 2, 6, 12, and 24 hr p.v. and disrupted in lysing matrix D 1.4-mm ceramic sphere tubes using FastPrep-24 tissue disruption (MP Biomedicals), and RNA was isolated using an RNAeasy Mini kit (QIAGEN). 1 μg of cDNA was synthesized using a cDNA synthesis kit (Applied Biosystems) following the manufacturer's recommendations. For the qPCR reaction, a SYBR Master Mix (Applied Biosystems) was used, and samples were run on a 7900HT Fast Real-Time PCR System (Applied Biosystems). Cytokine mRNA levels were expressed relative to GAPDH expression (primers: *GAPDH* forward, 5′-ACATCATCCCTGCATCCACT-3′; *GAPDH* reverse, 5′-AGATCCACGACGGACACATT-3′). The Pfaffl method (Pfaffl, 2001) was used to calculate the relative expression of the transcripts.

Multiphoton Microscopy and Analysis

Deep tissue imaging was performed on a customized two-photon platform (TrimScope, LaVision BioTec). Two-photon probe excitation and tissue second-harmonic generation (SHG) were obtained with a set of two tunable Ti:sapphire lasers (Chamaleon Ultra I, Chamaleon Ultra II, Coherent) and an optical parametric oscillator that emits in the range of 1,010 to 1,340 nm (Chamaleon Compact OPO, Coherent), with output wavelength in the range of 690–1,080 nm. The objectives used were a Nikon LWD 16×/0.80 numerical aperture (NA) W in Figure 1A and a Nikon N Plan Apo λ 4×/0.20 NA in Figure 5H. 3D reconstructions of whole popliteal LNs (Figure 1A) were made using a mosaic of up to 3 × 3 adjacent field-of-view image acquisitions with a z-depth of up to 300 μm. Images were stitched together using Fiji (Schindelin et al., 2012) together with a custom-developed script written in Beanshell to automate image processing. To automate the stitching operations, we developed a script using Beanshell programming language. The hyperstacks were subsequently imported in the software Imaris 7.7.2 (Bitplane) to obtain the 3D rendering of the LN. Cell populations were segmented (analysis in Figures 1B and 1C) by putting a threshold on the color intensity after background subtraction.

Statistics

All data are expressed as the mean ± SD. For statistical analyses and data representation, Prism 6.0b (GraphPad Software) was used. Group comparisons were assessed using nonparametric tests. All statistical test were two-tailed, and statistical significance was defined as $^*p < 0.05$, $^{**}p < 0.01$, and $^{***}p < 0.001$.

SUPPLEMENTAL INFORMATION

Supplemental Information includes four figures and one movie and can be found with this article online at http://dx.doi.org/10.1016/j.celrep.2017.02.026.

AUTHOR CONTRIBUTIONS

S.F.G. directed the study, designed experiments, analyzed and interpreted the results, and wrote the manuscript. N.C., Y.F., M.P.-S., R.D., D.U.P., and V.L.-K. designed and performed the experiment and analyzed results. F.S., M.U., D.C., S.J.T., A.L., and M.C.C. provided reagents and analyzed and interpreted results.

ACKNOWLEDGMENTS

We thank professors Harald von Boehmer and Shizuo Akira for providing influenza HA-specific CD4 TCR-α/β and MyD88 KO mice, respectively, and Maria Ericsson, Gabriela Danelon-Sargenti, Sara Cordeiro, and David Jarrossay for technical support. This work was supported by Swiss National Foundation (SNF) grants R'Equip (145038) and Ambizione (148183) and the Marie Curie Reintegration Grant 612742. S.F.G. was supported by a grant from the Swiss Vaccine Research Institute (SVRI). D.U.P. was supported by SystemsX.ch grant 2013/124.

Received: September 28, 2016
Revised: December 14, 2016
Accepted: February 7, 2017
Published: March 7, 2017

REFERENCES

Asselin-Paturel, C., Brizard, G., Chemin, K., Boonstra, A., O'Garra, A., Vicari, A., and Trinchieri, G. (2005). Type I interferon dependence of plasmacytoid dendritic cell activation and migration. J. Exp. Med. *201*, 1157–1167.

Barth, M.W., Hendrzak, J.A., Melnicoff, M.J., and Morahan, P.S. (1995). Review of the macrophage disappearance reaction. J. Leukoc. Biol. *57*, 361–367.

Carrasco, Y.R., and Batista, F.D. (2007). B cells acquire particulate antigen in a macrophage-rich area at the boundary between the follicle and the subcapsular sinus of the lymph node. Immunity *27*, 160–171.

Chen, C.J., Kono, H., Golenbock, D., Reed, G., Akira, S., and Rock, K.L. (2007). Identification of a key pathway required for the sterile inflammatory response triggered by dying cells. Nat. Med. *13*, 851–856.

Chtanova, T., Schaeffer, M., Han, S.J., van Dooren, G.G., Nollmann, M., Herzmark, P., Chan, S.W., Satija, H., Camfield, K., Aaron, H., et al. (2008). Dynamics of neutrophil migration in lymph nodes during infection. Immunity *29*, 487–496.

Clausen, B.E., Burkhardt, C., Reith, W., Renkawitz, R., and Förster, I. (1999). Conditional gene targeting in macrophages and granulocytes using LysMcre mice. Transgenic Res. *8*, 265–277.

Corti, D., Voss, J., Gamblin, S.J., Codoni, G., Macagno, A., Jarrossay, D., Vachieri, S.G., Pinna, D., Minola, A., Vanzetta, F., et al. (2011). A neutralizing antibody selected from plasma cells that binds to group 1 and group 2 influenza A hemagglutinins. Science *333*, 850–856.

Di Paolo, N.C., and Shayakhmetov, D.M. (2016). Interleukin 1α and the inflammatory process. Nat. Immunol. *17*, 906–913.

Diebold, S.S., Kaisho, T., Hemmi, H., Akira, S., and Reis e Sousa, C. (2004). Innate antiviral responses by means of TLR7-mediated recognition of single-stranded RNA. Science *303*, 1529–1531.

Eigenbrod, T., Park, J.H., Harder, J., Iwakura, Y., and Núñez, G. (2008). Cutting edge: critical role for mesothelial cells in necrosis-induced inflammation through the recognition of IL-1 alpha released from dying cells. J. Immunol. *181*, 8194–8198.

Farrell, H.E., Davis-Poynter, N., Bruce, K., Lawler, C., Dolken, L., Mach, M., and Stevenson, P.G. (2015). Lymph node macrophages restrict murine cytomegalovirus dissemination. J. Virol. *89*, 7147–7158.

Galluzzi, L., Bravo-San Pedro, J.M., Vitale, I., Aaronson, S.A., Abrams, J.M., Adam, D., Alnemri, E.S., Altucci, L., Andrews, D., Annicchiarico-Petruzzelli, M., et al. (2015). Essential versus accessory aspects of cell death: recommendations of the NCCD 2015. Cell Death Differ. *22*, 58–73.

Gaya, M., Castello, A., Montaner, B., Rogers, N., Reis e Sousa, C., Bruckbauer, A., and Batista, F.D. (2015). Host response. Inflammation-induced disruption of SCS macrophages impairs B cell responses to secondary infection. Science *347*, 667–672.

Gerner, M.Y., Torabi-Parizi, P., and Germain, R.N. (2015). Strategically localized dendritic cells promote rapid T cell responses to lymph-borne particulate antigens. Immunity *42*, 172–185.

Gonzalez, S.F., Lukacs-Kornek, V., Kuligowski, M.P., Pitcher, L.A., Degn, S.E., Kim, Y.A., Cloninger, M.J., Martinez-Pomares, L., Gordon, S., Turley, S.J., and Carroll, M.C. (2010). Capture of influenza by medullary dendritic cells via SIGN-R1 is essential for humoral immunity in draining lymph nodes. Nat. Immunol. *11*, 427–434.

Gray, E.E., and Cyster, J.G. (2012). Lymph node macrophages. J. Innate Immun. *4*, 424–436.

Hickman, H.D., Takeda, K., Skon, C.N., Murray, F.R., Hensley, S.E., Loomis, J., Barber, G.N., Bennink, J.R., and Yewdell, J.W. (2008). Direct priming of antiviral CD8+ T cells in the peripheral interfollicular region of lymph nodes. Nat. Immunol. *9*, 155–165.

Hou, B., Reizis, B., and DeFranco, A.L. (2008). Toll-like receptors activate innate and adaptive immunity by using dendritic cell-intrinsic and -extrinsic mechanisms. Immunity *29*, 272–282.

Iannacone, M., Moseman, E.A., Tonti, E., Bosurgi, L., Junt, T., Henrickson, S.E., Whelan, S.P., Guidotti, L.G., and von Andrian, U.H. (2010). Subcapsular sinus macrophages prevent CNS invasion on peripheral infection with a neurotropic virus. Nature *465*, 1079–1083.

Iwasaki, A., and Pillai, P.S. (2014). Innate immunity to influenza virus infection. Nat. Rev. Immunol. *14*, 315–328.

Jung, S., Aliberti, J., Graemmel, P., Sunshine, M.J., Kreutzberg, G.W., Sher, A., and Littman, D.R. (2000). Analysis of fractalkine receptor CX(3)CR1 function by targeted deletion and green fluorescent protein reporter gene insertion. Mol. Cell. Biol. *20*, 4106–4114.

Junt, T., Moseman, E.A., Iannacone, M., Massberg, S., Lang, P.A., Boes, M., Fink, K., Henrickson, S.E., Shayakhmetov, D.M., Di Paolo, N.C., et al. (2007). Subcapsular sinus macrophages in lymph nodes clear lymph-borne viruses and present them to antiviral B cells. Nature *450*, 110–114.

Kastenmüller, W., Torabi-Parizi, P., Subramanian, N., Lämmermann, T., and Germain, R.N. (2012). A spatially-organized multicellular innate immune response in lymph nodes limits systemic pathogen spread. Cell *150*, 1235–1248.

Kato, H., Sato, S., Yoneyama, M., Yamamoto, M., Uematsu, S., Matsui, K., Tsujimura, T., Takeda, K., Fujita, T., Takeuchi, O., and Akira, S. (2005). Cell type-specific involvement of RIG-I in antiviral response. Immunity *23*, 19–28.

Kirberg, J., Baron, A., Jakob, S., Rolink, A., Karjalainen, K., and von Boehmer, H. (1994). Thymic selection of CD8+ single positive cells with a class II major histocompatibility complex-restricted receptor. J. Exp. Med. *180*, 25–34.

Kuida, K., Lippke, J.A., Ku, G., Harding, M.W., Livingston, D.J., Su, M.S., and Flavell, R.A. (1995). Altered cytokine export and apoptosis in mice deficient in interleukin-1 beta converting enzyme. Science *267*, 2000–2003.

Kuka, M., and Iannacone, M. (2014). The role of lymph node sinus macrophages in host defense. Ann. N Y Acad. Sci. *1319*, 38–46.

Labow, M., Shuster, D., Zetterstrom, M., Nunes, P., Terry, R., Cullinan, E.B., Bartfai, T., Solorzano, C., Moldawer, L.L., Chizzonite, R., and McIntyre, K.W. (1997). Absence of IL-1 signaling and reduced inflammatory response in IL-1 type I receptor-deficient mice. J. Immunol. *159*, 2452–2461.

Lund, J.M., Alexopoulou, L., Sato, A., Karow, M., Adams, N.C., Gale, N.W., Iwasaki, A., and Flavell, R.A. (2004). Recognition of single-stranded RNA viruses by Toll-like receptor 7. Proc. Natl. Acad. Sci. USA *101*, 5598–5603.

Malmgaard, L., Melchjorsen, J., Bowie, A.G., Mogensen, S.C., and Paludan, S.R. (2004). Viral activation of macrophages through TLR-dependent and -independent pathways. J. Immunol. *173*, 6890–6898.

Mariathasan, S., Newton, K., Monack, D.M., Vucic, D., French, D.M., Lee, W.P., Roose-Girma, M., Erickson, S., and Dixit, V.M. (2004). Differential activation of the inflammasome by caspase-1 adaptors ASC and Ipaf. Nature *430*, 213–218.

Martín-Fontecha, A., Sebastiani, S., Höpken, U.E., Uguccioni, M., Lipp, M., Lanzavecchia, A., and Sallusto, F. (2003). Regulation of dendritic cell migration to the draining lymph node: impact on T lymphocyte traffic and priming. J. Exp. Med. *198*, 615–621.

Matsuki, T., Nakae, S., Sudo, K., Horai, R., and Iwakura, Y. (2006). Abnormal T cell activation caused by the imbalance of the IL-1/IL-1R antagonist system is responsible for the development of experimental autoimmune encephalomyelitis. Int. Immunol. *18*, 399–407.

Mempel, T.R., Henrickson, S.E., and Von Andrian, U.H. (2004). T-cell priming by dendritic cells in lymph nodes occurs in three distinct phases. Nature *427*, 154–159.

Merad, M., Sathe, P., Helft, J., Miller, J., and Mortha, A. (2013). The dendritic cell lineage: ontogeny and function of dendritic cells and their subsets in the steady state and the inflamed setting. Annu. Rev. Immunol. *31*, 563–604.

Moseman, E.A., Iannacone, M., Bosurgi, L., Tonti, E., Chevrier, N., Tumanov, A., Fu, Y.X., Hacohen, N., and von Andrian, U.H. (2012). B cell maintenance of subcapsular sinus macrophages protects against a fatal viral infection independent of adaptive immunity. Immunity *36*, 415–426.

Müller, U., Steinhoff, U., Reis, L.F., Hemmi, S., Pavlovic, J., Zinkernagel, R.M., and Aguet, M. (1994). Functional role of type I and type II interferons in antiviral defense. Science *264*, 1918–1921.

Pfaffl, M.W. (2001). A new mathematical model for relative quantification in real-time RT-PCR. Nucleic Acids Res. *29*, e45.

Phan, T.G., Grigorova, I., Okada, T., and Cyster, J.G. (2007). Subcapsular encounter and complement-dependent transport of immune complexes by lymph node B cells. Nat. Immunol. *8*, 992–1000.

Phan, T.G., Green, J.A., Gray, E.E., Xu, Y., and Cyster, J.G. (2009). Immune complex relay by subcapsular sinus macrophages and noncognate B cells drives antibody affinity maturation. Nat. Immunol. *10*, 786–793.

Rider, P., Carmi, Y., Guttman, O., Braiman, A., Cohen, I., Voronov, E., White, M.R., Dinarello, C.A., and Apte, R.N. (2011). IL-1α and IL-1β recruit different myeloid cells and promote different stages of sterile inflammation. J. Immunol. *187*, 4835–4843.

Roozendaal, R., Mempel, T.R., Pitcher, L.A., Gonzalez, S.F., Verschoor, A., Mebius, R.E., von Andrian, U.H., and Carroll, M.C. (2009). Conduits mediate transport of low-molecular-weight antigen to lymph node follicles. Immunity *30*, 264–276.

Sagoo, P., Garcia, Z., Breart, B., Lemaître, F., Michonneau, D., Albert, M.L., Levy, Y., and Bousso, P. (2016). In vivo imaging of inflammasome activation reveals a subcapsular macrophage burst response that mobilizes innate and adaptive immunity. Nat. Med. *22*, 64–71.

Schindelin, J., Arganda-Carreras, I., Frise, E., Kaynig, V., Longair, M., Pietzsch, T., Preibisch, S., Rueden, C., Saalfeld, S., Schmid, B., et al. (2012). Fiji: an open-source platform for biological-image analysis. Nat. Methods *9*, 676–682.

Seo, S.U., Kwon, H.J., Song, J.H., Byun, Y.H., Seong, B.L., Kawai, T., Akira, S., and Kweon, M.N. (2010). MyD88 signaling is indispensable for primary influenza A virus infection but dispensable for secondary infection. J. Virol. *84*, 12713–12722.

Staats, H.F., and Ennis, F.A., Jr. (1999). IL-1 is an effective adjuvant for mucosal and systemic immune responses when coadministered with protein immunogens. J. Immunol. *162*, 6141–6147.

Staudt, L.M., and Gerhard, W. (1983). Generation of antibody diversity in the immune response of BALB/c mice to influenza virus hemagglutinin. I. Significant variation in repertoire expression between individual mice. J. Exp. Med. *157*, 687–704.

Sung, J.H., Zhang, H., Moseman, E.A., Alvarez, D., Iannacone, M., Henrickson, S.E., de la Torre, J.C., Groom, J.R., Luster, A.D., and von Andrian, U.H. (2012). Chemokine guidance of central memory T cells is critical for antiviral recall responses in lymph nodes. Cell *150*, 1249–1263.

Winkelmann, E.R., Widman, D.G., Xia, J., Johnson, A.J., van Rooijen, N., Mason, P.W., Bourne, N., and Milligan, G.N. (2014). Subcapsular sinus macrophages limit dissemination of West Nile virus particles after inoculation but are not essential for the development of West Nile virus-specific T cell responses. Virology *450-451*, 278–289.

Woodruff, M.C., Heesters, B.A., Herndon, C.N., Groom, J.R., Thomas, P.G., Luster, A.D., Turley, S.J., and Carroll, M.C. (2014). Trans-nodal migration of resident dendritic cells into medullary interfollicular regions initiates immunity to influenza vaccine. J. Exp. Med. *211*, 1611–1621.

Cell Reports, Volume *18*

Supplemental Information

Macrophage Death following Influenza Vaccination Initiates the Inflammatory Response that Promotes Dendritic Cell Function in the Draining Lymph Node

Nikolaos Chatziandreou, Yagmur Farsakoglu, Miguel Palomino-Segura, Rocco D'Antuono, Diego Ulisse Pizzagalli, Federica Sallusto, Veronika Lukacs-Kornek, Mariagrazia Uguccioni, Davide Corti, Shannon J. Turley, Antonio Lanzavecchia, Michael C. Carroll, and Santiago F. Gonzalez

Supplementary Information: **Figure S1. Related to Figure 1:** Phenotypic characterization of SSM and MM.

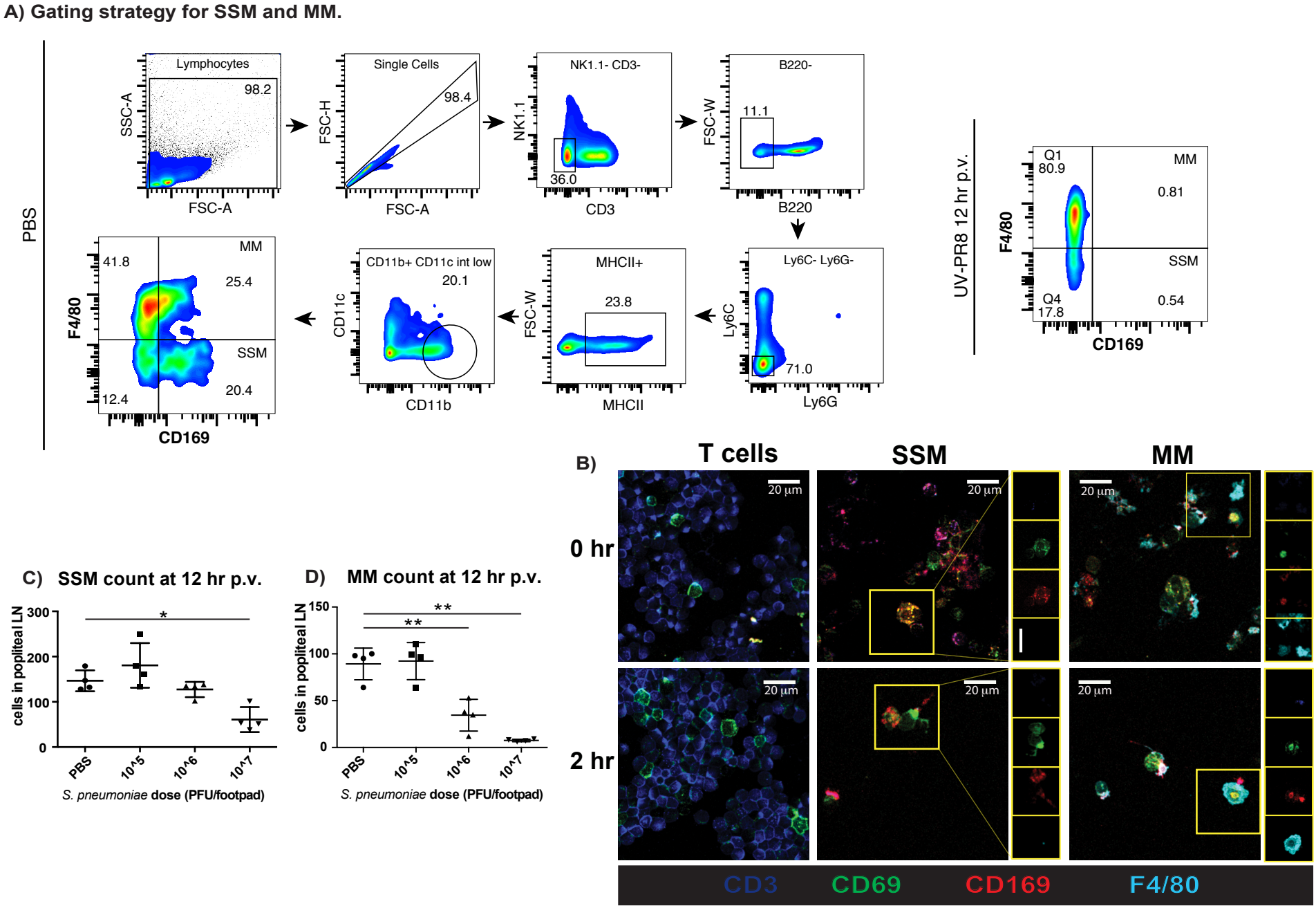

Figure S1, Related to Figure 1: A) Gating stategy for SSM and MM. Results from the PBS-treated control group (left) and vaccinated group at 12 hr p.v. (right) are shown. **B)** Confocal micrograph showing the expression of the surface markers CD3, CD69, CD169 and F4/80 in T cells, SSM and MM at 0 and 2 hr p.v. **C)** Flow cytometric analysis showing a correlation between the SSM and MM **(D)** dissapearance after vaccination with different dosages of heat-inactivated *Streptococcus pneumoniae*.

Figure S2. Related to Figure 2: Molecular characterization of SSM and MM necrotic death.

A) The inflammasome pathway is not involved in macrophage death.

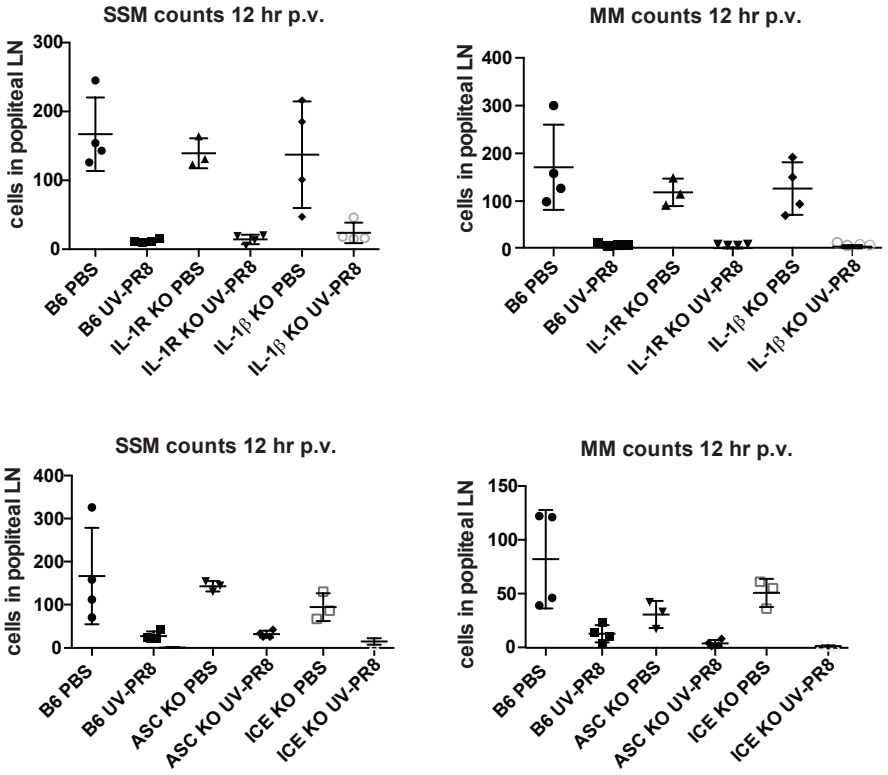

B) IL-1β and IL-18 expression levels p.v. (RQ-PCR)

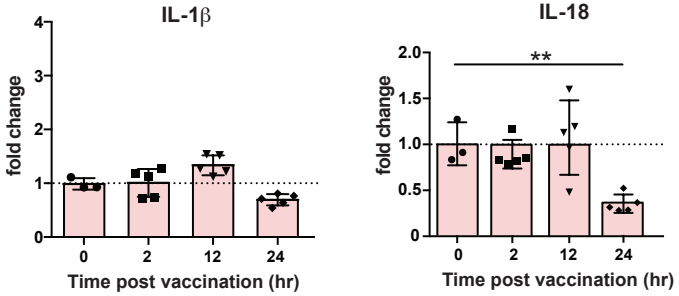

Macrophage disappearance is not associated with infiltrated inflammatory cells.

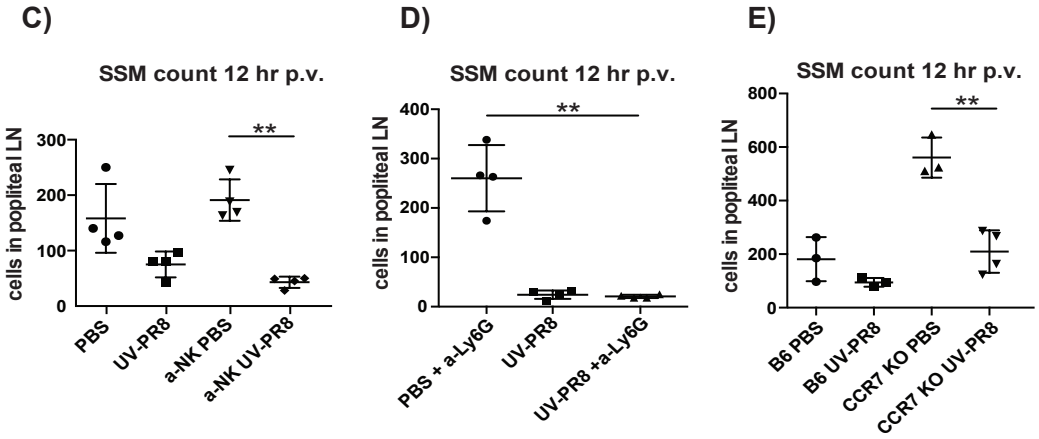

MM disappearance is induced by inflammation.

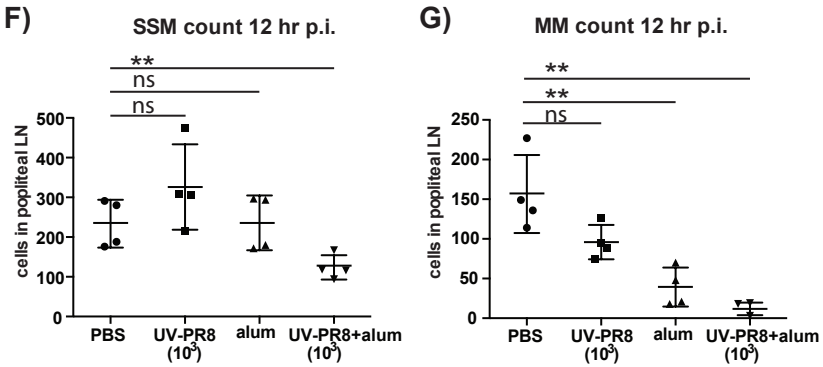

Figure S2, Related with Figure 2: (A) Flow cytometric analysis of SSM and MM from mice deficient in IL-1R, IL-1β, ASC and ICE at 12 hr p.v. showing that the inflammasome pathway is not involved in SSM and MM disappearance. **(B)** mRNA levels of the cytokines IL-1β and IL-18 measured in the popliteal LN at different times following vaccination. **C)** Flow cytometric analysis of SSM disappearance in mice pre-treated with NK-depleting antibody (a-NK) neutrophil-depleting antibody (a-Ly6G) **(D)** or CCR7 KO **(E)** compared with untreated controls. **(F)** Flow cytometric analysis showing the effect of administration of alum alone or together with a low viral dose (10^3 PFU) in SSM and MM at 12 hr post injection **(G)**. Presented data are representative of at least three independent experiments with n ≥ 3. *, P< 0.1; **, P< 0.01; ***, P< 0.001.

Figure S3. Related to Figure 5: Constitutive expression of IFN-β and IL-1α in LN.

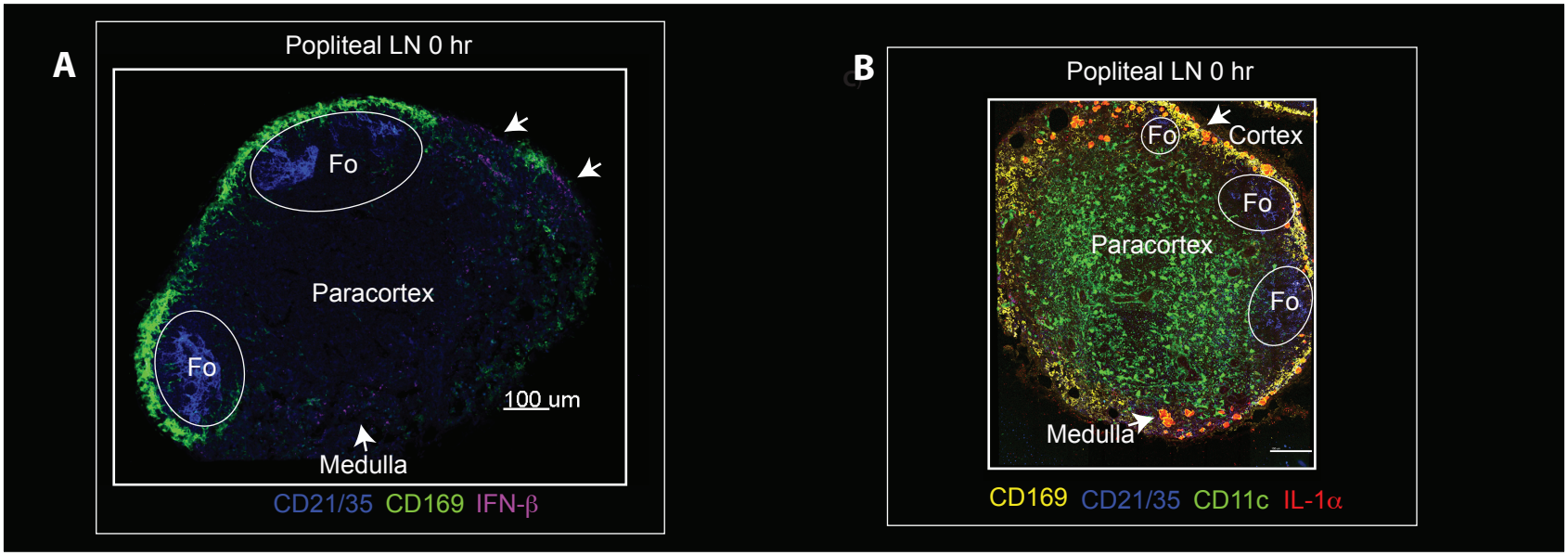

Figure S3. Related to Figure 5: Representative confocal micrographs showing the constitutive expression of IFN-β (**A**) and IL-1α (**B**) in the popliteal LN (white arrows) which is associated with LN macrophages. Presented data are representative of at least three independent experiments with n ≥ 3. Fo stands for B cell follicle.

Figure S4. Related to Figure 6: Phenotypic characterization of LNDC.

A) Gating strategy for LN DC subsets.

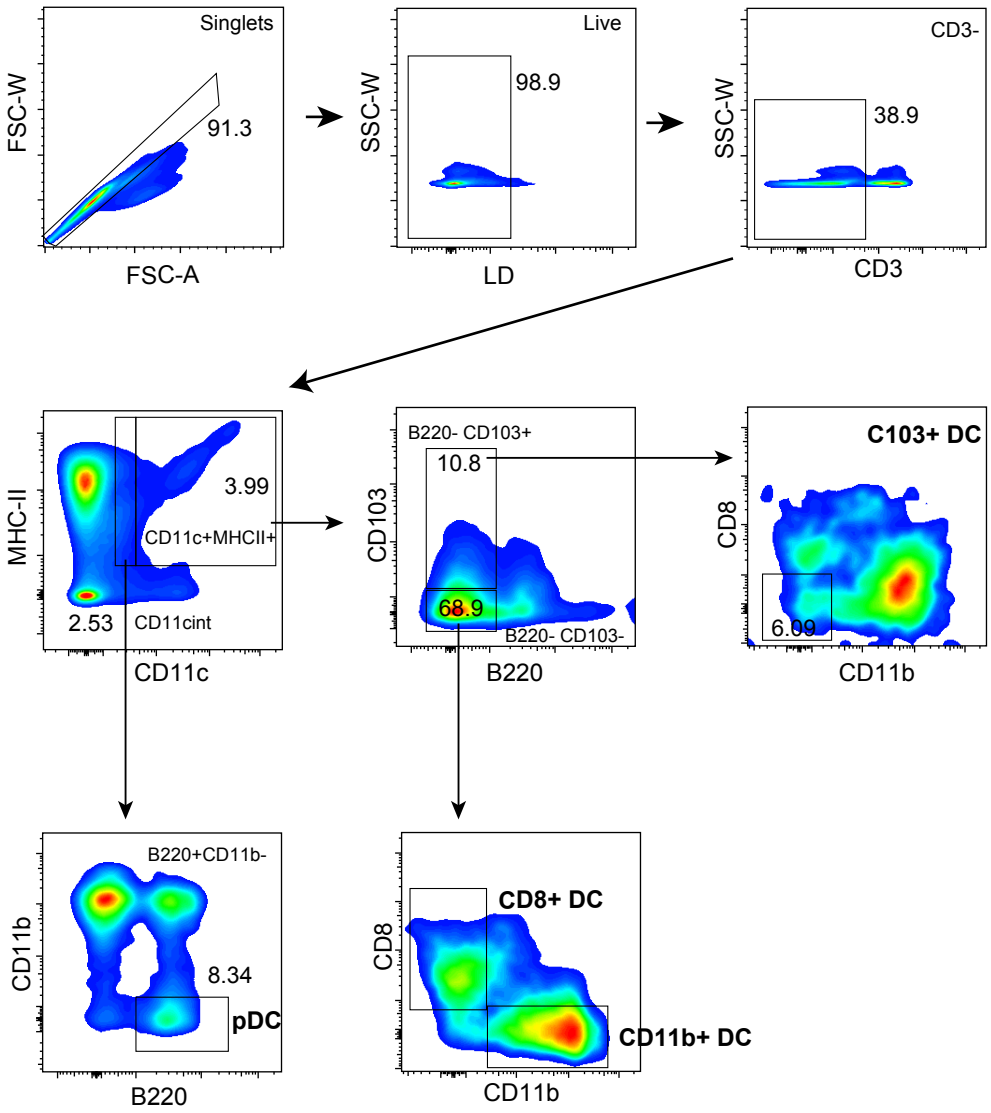

B) Upregulation of CCR2 in CD11b+ DC.

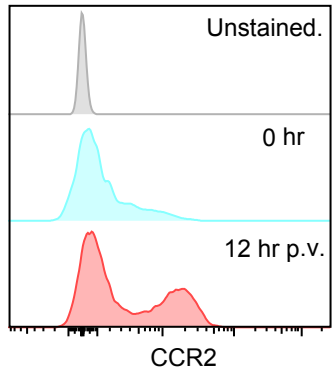

C) IFN expression associated to LNM is necessary for DC activation.

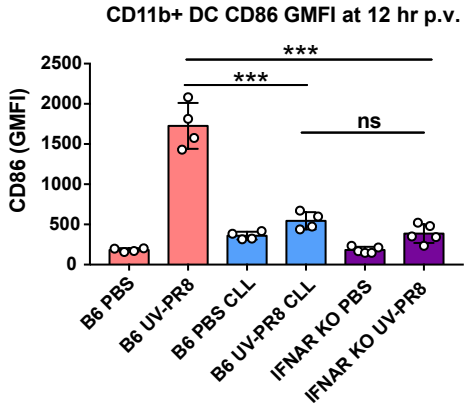

Figure S4. Related to Figure 6: A) Gating stategy for the LN DC subsets: CD103+DC, pDC, CD11b+DC and CD8+DC. **B)** Histogram showing the upregulation of CCR2 in CD11b+ DC at 12 hr p.v. **C)** GMFI analysis showing differences in the expression of the costimulatory molecule CD86 in the presence or absence of LN macrophages or interferon receptor at 12 hr p.v.***,P<0.001, NS stands for non significant.

Movie S1. **Related to Figure 1:** LN macrophages undergo cell death following influenza vaccination.

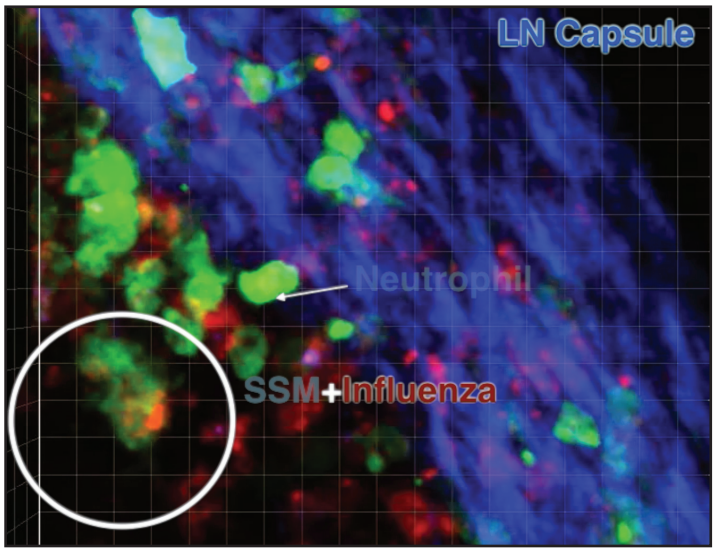

Movie S1. Related with Figure 1: 2-photon intravital movie of a popliteal LN starting at 12 hr p.v. Subcapsular sinus macrophages (larger static green cells) capture inactivated influenza virus (red). The white circle shows a SSM undergoing necrosis, leaving behind the internalized virus. Additionally, neutrophils (smaller motile green cells) interact closely with necrotic macrophages capturing viral particles.